An efficient diffusion generated motion method for wetting dynamics

Song Lu [1] , Xianmin Xu[2]
LSEC, ICMSEC, NCMIS, Academy of Mathematics and Systems Science, Chinese Academy of Sciences, Beijing 100190, China;
School of Mathematical Sciences, University of Chinese Academy of Sciences, Beijing 100049, China

Abstract

By using the Onsager variational principle as an approximation tool, we develop a new diffusion generated motion method for wetting problems. The method uses a signed distance function to represent the interface between the liquid and vapor surface. In each iteration, a linear diffusion equation with a linear boundary condition is solved for one time step in addition to a simple re-distance step and a volume correction step. The method has a first-order convergence rate with respect to the time step size even in the vicinity three-phase contact points. Its energy stability property is analysed by careful studies for some geometric flows on substrates. Numerical examples show that the method can be used to simulate complicated wetting problems on inhomogeneous surfaces.

1. Introduction

Wetting describes how liquid stays and spreads on solid surfaces. It is a fundamental two-phase flow problem and has important applications in many industrial processes, e.g. in coating, printing, oil industry, etc. When the solid surface is homogeneous, the contact angle between the liquid surface and the substrate is characterized by Young's equation[1]. However, when the solid surface is chemically inhomogeneous or geometrically rough, the wetting phenomena become much more complicated. The apparent contact angle may be very different from Young's angle(so-called the lotus effect). There also exist many meta-stable states in the solid-liquid-vapor system, and this generates the interesting contact angle hysteresis phenomenon. Many theoretical and experimental studies have been done for the wetting problems(c.f. [2, 3, 4] and many references therein).

Mathematically, wetting is a free interface problem with complicated boundary conditions. A liquid drop can change shape or even topology on a solid substrate. On the contact line, which is the line between the liquid-vapor interface and the solid surface, Young's equation holds locally. Numerical simulation for the wetting problem is very challenging, especially for that on rough or chemically inhomogeneous surfaces. The standard methods based on a sharp-interface representation of the liquid-vapor interface are difficult to deal with the topology change and the complicated boundary conditions [5, 6, 7, 8, 9]. On the other hand, the diffuse-interface model for the wetting problem includes a nonlinear relaxed boundary condition[10, 11], which is also difficult to deal with numerically. Moreover, in comparison with the phase-field model in other applications, one needs a very small interface thickness parameter in wetting problems, since the parameter must be much smaller than the characteristic size of the roughness or chemical inhomogeneity in order to simulate the wetting phenomena correctly.

Recently, a threshold dynamics method has been developed for wetting problems on rough surfaces[12, 13]. The method alternately diffuses and sharpens a linear combination of the characteristic functions of the liquid, the vapor and the solid domains to decrease the total interfacial energy of the three-phase system.

[1]lusong@lsec.cc.ac.cn.
[2]Corresponding author. xmxu@lsec.cc.ac.cn.

The method is efficient since in each iteration one needs only to solve one or two linear diffusion equations in addition to a simple thresholding step and a volume correction step. The diffusion equation can be solved by standard FFT method or non-uniform FFT techniques[14, 15]. However, the accuracy of the method is not very satisfactory, since one can only obtain a convergence rate of half order with respect to the time step δt(i.e. of order $O(\delta t^{1/2})$) near the three-phase contact points. This is crucial in wetting problems since it is the contact angle condition at these points that determines the main physical properties of wetting. To compute the wetting problem correctly, one usually needs to choose a very small time step size and very fine meshes, especially for rough or chemically inhomogeneous surfaces.

The threshold dynamic method for wetting in [12, 13] is basically an MBO type method[16, 17, 18] and can be seen as a generalization of the method recently developed in [19]. This method has been studied a lot and also been used in many different problems [20, 21, 22, 23, 24]. One can also employ signed distance functions to replace the characteristic functions in some applications[25, 26]. Main advantages of these methods are that they are easy to implement and can deal with the topological changes naturally. A disadvantage is that the accuracy of the method is not very good for multi-phase free interface problems with a triple junction. In general, the convergence rate with respect to the time step of the method is of order $O(\delta t)$ for smooth curves while it is of order $O(\delta t^{1/2})$ when there is a triple junction[27]. Some second-order threshold dynamics schemes have been developed for smooth curves in [17, 28]. However, it is not clear if the methods work for multi-phase problems with triple junctions.

In this paper, we develop a new diffusion generalized method using the signed distance function for wetting problems. The method is efficient and easy to implement, since like in the standard method, in each iteration, the main step is to solve a linear diffusion equation with a linear boundary condition. Meanwhile, the method achieves a first-order convergence rate $O(\delta t)$ with respect to the time step even near three-phase contact points. The main difference of the method from the previous ones in [12, 13] is that we do not include the solid phase domain in the diffusion equation. Therefore the three-phase contact points are not inside the computational domain but on the boundary and the corresponding contact angle conditions can be approximated with higher accuracy.

Another novelty of our work is that we use the Onsager principle[29, 30, 31] as an approximation tool to derive a linear diffusion equation with a linear boundary condition for the liquid-vapor interface, which is the main equation to be solved in the proposed numerical method. The Onsager Principle is a fundamental variational principle in statistic physics[30, 29, 31]. Recently, it is found that the principle can be used as a powerful approximation tool in many problems in soft matter [32, 33, 34, 35, 36, 37, 38, 39]. We use the idea in a novel way to derive the linear equation for wetting problems. This is done by assuming a *tanh* profile of the leading order approximation of a phase-field model for wetting problems and choosing the signed distance function of the liquid-vapor interface as an unknown function. By applying the Onsager principle, we show that the signed distance function approximately satisfies a linear diffusion equation with a simple linear boundary condition.

We also give a stability analysis for the proposed method. The analysis is based on an approximation of the method by some geometric flows and careful studies of their geometric properties. We show that the total wetting energies decay when the time step is small. Under some conditions for the geometric flows, we can relax the constraint of the small time step in the analysis. Numerical examples show that the method works well for wetting problems on chemically inhomogeneous surfaces. The contact angle hysteresis phenomena can be computed correctly.

The rest part of the paper is organized as follows. In section 2, we give the Onsager principle briefly and the main idea to use it as an approximation tool. In section 3, we introduce the mathematical models for wetting problems. In particular, we show that the Onsager principle can be used to derive a modified Allen-Cahn equation with a relaxed boundary condition. In section 4, we derive a linear diffusion equation for the signed distance function of the liquid-vapor interface by using the Onsager principle to approximate the modified Allen-Cahn equation. The diffusion equation is then used to construct a diffusion generated motion method for wetting problems. In section 5, we give some analysis of the energy stability property of our method. In section 6, some numerical examples are given to show the method has a first-order convergence rate and works well for wetting problems on chemically inhomogeneous surfaces. Finally, some concluding remarks are given in the last section.

2. The Onsager Principle as an approximation tool

The Onsager Principle is a variational principle in statistic physics[30, 29]. It has been used to derive models in many problems in soft matter science, such as the Stokes equation in hydrodynamics, the generalized Navier slip boundary condition in moving contact line problems, the Nernst-Planck equation in electro-kinetics, the Ericksen-Leslie equation in nematic liquid crystals, etc [31, 40, 41]. We will introduce it briefly in this section and more details are referred to [31].

Suppose a non-equilibrium physical system is characterized by a set of parameters α_i, $i = 1, \cdots, M$, which may depend both on space and time. When the inertial effect is ignored, the dynamics of the parameters can be determined by using the Onsager principle as follows. Firstly, define the Rayleignian function in the system with respect to $\dot{\alpha} = \{\dot{\alpha}_1, \cdots, \dot{\alpha}_M\}$, which is the changing rate of the parameter α, as

$$\mathcal{R}(\alpha; \dot{\alpha}) = \Phi(\dot{\alpha}) + \dot{\mathcal{E}}(\alpha; \dot{\alpha}), \tag{1}$$

where $\Phi(\dot{\alpha})$ is the energy dissipation function, which is the half of the total energy dissipation rate in the system, and $\dot{\mathcal{E}}(\alpha, \dot{\alpha})$ is the changing rate of total energy $\mathcal{E}(\alpha)$. In general, the energy dissipation function can be written as a quadratic form of $\dot{\alpha}$, i.e.,

$$\Phi(\dot{\alpha}) = \frac{1}{2} \sum_{i,j=1}^{M} \zeta_{ij} \dot{\alpha}_i \dot{\alpha}_j,$$

where ζ_{ij} is a symmetric positive matrix. Here we ignore the spacial integration for simplicity. Then the dynamics of α_i, $i = 1, \cdots, M$ can be determined by minimizing the total Rayleignian with respect to $\dot{\alpha}$, namely

$$\min_{\dot{\alpha}} \mathcal{R}(\alpha; \dot{\alpha}). \tag{2}$$

This leads to a dynamic equation for α,

$$\sum_{j=1}^{M} \zeta_{ij} \dot{\alpha}_j = -\frac{\delta \mathcal{E}}{\delta \alpha_i}. \tag{3}$$

The equation is actually the Euler-Lagrange equation for (2). In the next section, we will use the principle to derive a modified Allen-Cahn equation for the wetting problem.

Recently, it is found that the principle can be used as a powerful approximation tool[32, 33, 34, 35]. The key idea is to use Onsager principle only for a few key parameters(not the whole set α) which describe the system approximately. If the selected parameters depend only on time, then we derive an ordinary differential equation for them. In general, the ODE equation is much easier to solve than (3) but still captures the main properties of the complicated physical system. This method is very useful to approximate many free boundary problems in two-phase flows, visco-elastic fluids, etc [33, 34, 37, 38]. In section 4, we will use the idea to derive an efficient numerical method for wetting problems.

3. Mathematical models of the wetting problem

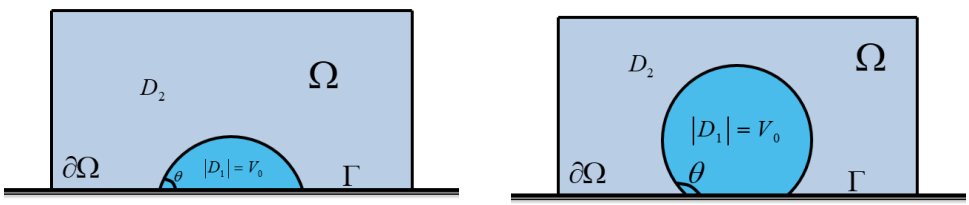

Figure 1: Wetting phenomena: a droplet on a hydrophilic substrate(left) and that on a hydrophobic one(right)

3.1. The sharp-interface model

In wetting problems, if one ignores the gravity, the total energy of a liquid-vapor-solid system is composed of three interface energies, i.e.

$$\mathcal{E} = \gamma_{LV}|\Sigma_{LV}| + \gamma_{SL}|\Sigma_{SL}| + \gamma_{SV}|\Sigma_{SV}|. \tag{4}$$

where γ_{LV}, γ_{SL} and γ_{SV} are respectively the energy densities of the liquid-vapor interface Σ_{LV}, the solid-liquid interface Σ_{SL} and the solid-vapor interface Σ_{SV}. The stationary profile of a liquid droplet on a solid surface is determined by minimizing the total energy under the constraint that the volume of the droplet is fixed.

To specify the mathematical model, we suppose the liquid domain is $D_1 \subset \Omega$ and the vapor domain is $D_2 = \Omega \setminus D_1$, as shown in Figure 1. The solid surface Γ is the lower boundary of Ω. The liquid-vapor interface is given by $\Sigma_{LV} = \partial D_1 \cap \partial D_2$, the solid-liquid interface is $\Sigma_{SL} = \partial D_1 \cap \Gamma$ and the solid-vapor interface is $\Sigma_{SV} = \partial D_2 \cap \Gamma$. Then the mathematical problem of wetting is

$$\min_{D_1 \cup D_2 = \Omega, |D_1| = V_0} \mathcal{E}(D_1, D_2) := \gamma_{LV}|\partial D_1 \cap \partial D_2| + \int_{\partial D_1 \cap \Gamma} \gamma_{SL}(s)\mathrm{d}s + \int_{\partial D_2 \cap \Gamma} \gamma_{SV}(s)\mathrm{d}s. \tag{5}$$

Here we write the surface energy on the solid boundary Γ into an integral since the energy densities γ_{SL} and γ_{SV} might not be constant when the solid surface is chemically inhomogeneous.

When the solid surface is planar and homogeneous, the energy minimizing problem (5) has a unique minimizer corresponding to a spherical droplet with a contact angle, which is the angle between the liquid-vapor interface and the solid surface, given by Young's equation[1]:

$$\gamma_{LV} \cos\theta_Y = \gamma_{SV} - \gamma_{SL}. \tag{6}$$

When the solid substrate is geometrically rough or chemically inhomogeneous, there are many local minimizers for the problem (5). The corresponding Euler-Lagrange equation is a free boundary problem with multi-scale boundary conditions, in which the microscopic inhomogeneity affects the apparent contact angle dramatically. Both analysis and numerical simulations are difficult for the wetting problem on a rough or chemically inhomogeneous surface.

The problem (5) can be rewritten into an equivalent form. Denote $C_0 = \frac{1}{2}\int_\Gamma \gamma_{SL}(s) + \gamma_{SV}(s)\mathrm{d}s$ as a constant depending only on the property of the solid boundary Γ. The total wetting energy is rewritten as

$$\begin{aligned}\mathcal{E}(D_1, D_2) &= \gamma_{LV}|\partial D_1 \cap \partial D_2| + \int_{\partial D_1 \cap \Gamma} \frac{\gamma_{SL}(s) - \gamma_{SV}(s)}{2}\mathrm{d}s + \int_{\partial D_2 \cap \Gamma} \frac{\gamma_{SV}(s) - \gamma_{SL}(s)}{2}\mathrm{d}s + C_0 \\ &= \gamma_{LV}|\partial D_1 \cap \partial D_2| - \frac{\gamma_{LV}}{2}\int_{\partial D_1 \cap \Gamma} \cos\theta_Y(s)\mathrm{d}s + \frac{\gamma_{LV}}{2}\int_{\partial D_2 \cap \Gamma} \cos\theta_Y(s)\mathrm{d}s + C_0. \end{aligned} \tag{7}$$

Here we have used Young's equation (6) and regard $\theta_Y(s)$ as a property of the substrate. Then the problem (5) is equivalent to the following one

$$\min_{D_1 \cup D_2 = \Omega, |D_1| = V_0} \tilde{\mathcal{E}}(D_1, D_2) := \sigma|\partial D_1 \cap \partial D_2| - \frac{\sigma}{2}\int_{\partial D_1 \cap \Gamma} \cos\theta_Y(s)\mathrm{d}s + \frac{\sigma}{2}\int_{\partial D_2 \cap \Gamma} \cos\theta_Y(s)\mathrm{d}s, \tag{8}$$

where σ is a given positive parameter, which can be seen as a dimensionless surface tension.

3.2. The phase-field model

Since the sharp-interface model described above is difficult in analysis and numerical simulations, it is convenient to consider a phase-field approximation for the problem (8). The idea is to use a smooth phase field function ϕ_ε to approximate the liquid-vapor interface $\partial D_1 \cap \partial D_2$ [42]. The total interface energy in (8) can be approximated by

$$\mathcal{E}_\varepsilon(\phi_\varepsilon) = \int_\Omega \frac{\varepsilon}{2}|\nabla\phi_\varepsilon|^2 + \frac{1}{\varepsilon}f(\phi_\varepsilon)\mathrm{d}x + \int_\Gamma g(\phi_\varepsilon)\mathrm{d}s, \tag{9}$$

where $f(\phi_\varepsilon) = \frac{(1-\phi_\varepsilon^2)^2}{4}$ and $g(\phi_\varepsilon) = -\frac{\sigma}{4}\cos\theta_Y(s)(3\phi_\varepsilon - \phi_\varepsilon^3)$ with $\sigma = \frac{2\sqrt{2}}{3}$. The phase-field model for the stationary wetting problem is

$$\inf_{\int_\Omega \phi_\varepsilon dx = C_1} \mathcal{E}_\varepsilon(\phi_\varepsilon). \tag{10}$$

Here C_1 is a given constant to make sure the volume of the liquid domain $|\{x|\phi_\varepsilon(x) > 0\}| = V_0$. It has been shown that the energy functional $\mathcal{E}_\varepsilon$ Γ-converges to the sharp-interface energy $\tilde{\mathcal{E}}$ defined in (8) when ε goes to zero [43, 11]. Hereinafter we use ϕ instead of ϕ_ε for simplicity in notations.

3.3. Derivation of a modified Allen-Cahn equation by the Onsager principle

We will use the Onsager principle to derive a gradient flow equation for the phase-field model (10). For that purpose, we define the energy dissipation function, which is the half of total energy dissipation rate, as follows

$$\Phi = \frac{1}{2}\int_\Omega \dot{\phi}^2 \mathrm{d}x + \frac{\xi}{2}\int_\Gamma \dot{\phi}^2 \mathrm{d}s. \tag{11}$$

Here $\xi \geq 0$ is a phenomenological parameter and we use $\dot{\phi} = \partial_t \phi$ for simplicity in notation. The function Φ includes the dissipation in the bulk domain and also that on the boundary when $\xi > 0$. The Rayleighian is given by

$$\mathcal{R}(\phi; \dot{\phi}) = \Phi(\dot{\phi}) + \dot{\mathcal{E}}_\varepsilon(\phi; \dot{\phi}), \tag{12}$$

where $\dot{\mathcal{E}}_\varepsilon$ is the changing rate of the total potential energy $\mathcal{E}_\varepsilon$. By integration by part, we have

$$\dot{\mathcal{E}}_\varepsilon(\phi; \dot{\phi}) = \int_\Omega (-\varepsilon\Delta\phi + \varepsilon^{-1} f'(\phi))\dot{\phi}\mathrm{d}x + \int_\Gamma (\varepsilon\partial_n\phi + g'(\phi))\dot{\phi}\mathrm{d}s + \int_{\partial\Omega\setminus\Gamma} \varepsilon(\partial_n\phi)\dot{\phi}\mathrm{d}s. \tag{13}$$

By the Onsager principle, a dynamic equation for ϕ can be derived by minimizing the Rayleighian $\mathcal{R}(\phi; \dot{\phi})$ with respect to $\dot{\phi}$ under the constraint that $\int_\Omega \phi \mathrm{d}x = C_1$. Notice that this condition is equivalent to $\int_\Omega \dot{\phi}\mathrm{d}x = 0$ since the initial value $\phi(x, 0)$ satisfies $\int_\Omega \phi(x, 0)\mathrm{d}x = C_1$. Therefore, the dynamic equation is determined by the variational problem

$$\min_{\int_\Omega \dot{\phi}\mathrm{d}x = 0} \mathcal{R}(\phi; \dot{\phi}). \tag{14}$$

By introducing a Lagrangian multiplier λ, we obtain a modified functional

$$\mathcal{R}_\lambda = \mathcal{R} - \lambda\int_\Omega \dot{\phi}\mathrm{d}x = \Phi + \dot{\mathcal{E}}_\varepsilon - \lambda\int_\Omega \dot{\phi}\mathrm{d}x.$$

Direct computations for the Fréchet derivative with respect to $\dot{\phi}$ give

$$\langle \frac{\delta\mathcal{R}_\lambda}{\delta\dot{\phi}}, \psi\rangle = \int_\Omega (\dot{\phi} - \varepsilon\Delta\phi + \varepsilon^{-1}f'(\phi) - \lambda)\psi\mathrm{d}x + \int_\Gamma (\xi\dot{\phi} + \varepsilon\partial_n\phi + g'(\phi))\psi\mathrm{d}s + \int_{\partial\Omega\setminus\Gamma} \varepsilon(\partial_n\phi)\psi\mathrm{d}s.$$

The Euler-Lagrange equation of (14) is given by

$$\begin{cases} \langle \frac{\delta\mathcal{R}_\lambda}{\delta\dot{\phi}}, \psi\rangle = 0, & \forall\psi; \\ \frac{\delta\mathcal{R}_\lambda}{\delta\lambda} = 0; \end{cases} \tag{15}$$

which leads to a modified Allen-Cahn equation,

$$\begin{cases} \partial_t\phi - \varepsilon\Delta\phi + \varepsilon^{-1}f'(\phi) = \lambda, & \text{in } \Omega; \\ \xi\partial_t\phi + \varepsilon\partial_n\phi + g'(\phi) = 0, & \text{on } \Gamma; \\ \partial_n\phi = 0, & \text{on } \partial\Omega\setminus\Gamma; \\ \int_\Omega \phi dx = C_1. \end{cases} \tag{16}$$

Here $f'(\phi) = \phi^3 - \phi$ and $g'(\phi) = -\frac{3\sigma}{4}\cos\theta_Y(1-\phi^2) = -\frac{\sqrt{2}}{2}(1-\phi^2)\cos\theta_Y$. Notice that when $\xi > 0$, the second equation in (16) is a dynamic relaxed boundary condition as in [10, 44]. When $\xi = 0$, it is a standard Neumann boundary condition.

By the above derivation, we can easily see the energy decay property of the solution of the Allen-Cahn equation (16). Suppose that ϕ is the solution of the modified Allen-Cahn equation (16). By the equations (16), (13), (15) and $\int_\Omega \dot{\phi} dx = 0$, we have

$$\begin{aligned}\frac{d\mathcal{E}_\varepsilon}{dt} &= \int_\Omega (-\varepsilon\Delta\phi + \varepsilon^{-1}f'(\phi))\dot{\phi}\mathrm{d}x + \int_{\partial\Omega}(\varepsilon\partial_n\phi + g'(\phi))\dot{\phi}ds + \int_{\partial\Omega\setminus\Gamma}\varepsilon(\partial_n\phi)\dot{\phi}\mathrm{d}s \\ &= \int_\Omega(-\dot{\phi}+\lambda)\dot{\phi}\mathrm{d}x - \xi\int_\Gamma \dot{\phi}^2\mathrm{d}s = -\int_\Omega \dot{\phi}^2\mathrm{d}x - \xi\int_\Gamma\dot{\phi}^2\mathrm{d}s \le 0.\end{aligned}$$

Therefore, when t goes to infinity, the stationary solution of the Allen-Cahn equation corresponds to a minimizer of the problem (10).

The modified equation (16) is more difficult to solve numerically than the standard Allen-Cahn equation, since we have a nonlinear boundary condition on the solid boundary in the second equation of (16). The boundary condition implies that the contact angle of the liquid is relaxed to or equal to the local Young's angle. In addition, the last equation of (16) provides a non-local constraint for the phase-field function. The boundary condition is different from the standard dynamic boundary condition for Allen-Cahn equation in literature[45, 46, 47, 48, 49], but similar to that for contact line motion in [10, 44, 50].

4. A diffusion generated motion method

To obtain the equilibrium state of the wetting problem, one can solve the modified Allen-Cahn equation (16) by some standard numerical methods(e.g. [51, 52]). However, when the parameter ε is small, the equation is very difficult to solve. Here we will not solve the equation directly. Instead, we will use it to develop an efficient diffusion generated motion method for the wetting problem (8). The key idea is to use the Onsager Principle as a tool to approximate the Allen-Cahn equation.

4.1. Approximation of an Allen-Cahn equation by using the Onsager Principle.

In this subsection, we ignore the non-local constraint $\int_\Omega \phi dx = C_1$ in the phase field equation (16). The constraint comes from the volume conservation condition of the wetting problem (8) and will be considered in next subsection. We consider an Allen-Cahn equation

$$\begin{cases} \partial_t\phi - \varepsilon\Delta\phi + \varepsilon^{-1}f'(\phi) = 0, & \text{in } \Omega; \\ \xi\partial_t\phi + \varepsilon\partial_n\phi + g'(\phi) = 0, & \text{on } \Gamma; \\ \partial_n\phi = 0, & \text{on } \partial\Omega\setminus\Gamma. \end{cases} \tag{17}$$

Similar to the analysis in the previous section, it is easy to see that the equation (17) can be derived by using the Onsager principle for the Reighleignian (12). In the following, we will use the Onsager principle to do some approximations for the equation (17).

Since ε is a small parameter, standard asymptotic analysis (c.f. [53, 11]) implies that the solution of (17) can be expanded with respect to ε as

$$\phi(x,t) = \phi_0(x,t) + \varepsilon\phi_1(x,t) + \cdots,$$

where $\phi_0(x,t) = \tanh(\frac{d(x,t)}{\sqrt{2}\varepsilon})$ and $d(x,t)$ is a signed distance function with respect to the zero level set of $\phi_0(x,t)$ such that $d(x,t) > 0$ when $\phi_0(x,t) > 0$. Here the boundary condition in (17) does not affect the leading order approximation since $g(\phi)$ has been properly chosen to match the expansions in bulk as shown in [11, 44]. When we are interested only in the leading order approximation of ϕ, we can assume

$$\phi(x,t) \approx \phi_0(x,t) = \Psi\Big(\frac{d(x,t)}{\sqrt{2}\varepsilon}\Big) := \tanh\Big(\frac{d(x,t)}{\sqrt{2}\varepsilon}\Big). \tag{18}$$

In this approximation, the only unknown is the signed distance function $d(x,t)$ with respect to the zero level set of ϕ_0.

We now derive a dynamic equation for the signed distance function $d(x,t)$ by using the Onsager Principle. It is easy to see that $\Psi'(\cdot) = 1 - \Psi^2(\cdot)$. Direct calculations give

$$\nabla\phi \approx \frac{1}{\sqrt{2}\varepsilon}\Psi'\Big(\frac{d(x,t)}{\sqrt{2}\varepsilon}\Big)\nabla d = \frac{1}{\sqrt{2}\varepsilon}\Big(1-\Psi^2\Big(\frac{d(x,t)}{\sqrt{2}\varepsilon}\Big)\Big)\nabla d = \frac{1}{\sqrt{2}\varepsilon}(1-\phi_0^2)\nabla d,$$
$$\partial_t\phi \approx \frac{1}{\sqrt{2}\varepsilon}\Psi'\Big(\frac{d(x,t)}{\sqrt{2}\varepsilon}\Big)\partial_t d = \frac{1}{\sqrt{2}\varepsilon}\Big(1-\Psi^2\Big(\frac{d(x,t)}{\sqrt{2}\varepsilon}\Big)\Big)\partial_t d = \frac{1}{\sqrt{2}\varepsilon}(1-\phi_0^2)\partial_t d.$$

Combing the above approximations with (18), the energy dissipation function (defined in (11)) in the system can be calculated as

$$\Phi \approx \frac{1}{4\varepsilon^2}\int_\Omega (1-\phi_0^2)^2(\partial_t d)^2 \mathrm{d}x + \frac{\xi}{4\varepsilon^2}\int_\Gamma (1-\phi_0^2)^2(\partial_t d)^2\mathrm{d}s \tag{19}$$
$$= \frac{1}{\varepsilon^2}\int_\Omega f(\phi_0)(\partial_t d)^2\mathrm{d}x + \frac{\xi}{\varepsilon^2}\int_\Gamma f(\phi_0)(\partial_t d)^2\mathrm{d}s. \tag{20}$$

Similar calculations for the total free energy(defined in (9)) lead to

$$\mathcal{E}_\varepsilon \approx \int_\Omega \frac{1}{\varepsilon} f(\phi_0)(|\nabla d(x,t)|^2+1)\mathrm{d}x + \int_\Gamma g(\phi_0)\mathrm{d}s. \tag{21}$$

The time derivative of $\mathcal{E}_\varepsilon$ is calculated by

$$\begin{aligned}
\dot{\mathcal{E}}_\varepsilon &\approx \int_\Omega \frac{2}{\varepsilon} f(\phi_0)\nabla d\cdot\nabla\partial_t d + \frac{(1+|\nabla d|^2)}{\varepsilon}f'(\phi_0)\Psi'\Big(\frac{d(x,t)}{\sqrt{2}\varepsilon}\Big)\frac{\partial_t d}{\sqrt{2}\varepsilon}\mathrm{d}x + \int_\Gamma g'(\phi_0)\Psi'\Big(\frac{d(x,t)}{\sqrt{2}\varepsilon}\Big)\frac{\partial_t d}{\sqrt{2}\varepsilon}\mathrm{d}s\\
&= \int_\Omega -\frac{2}{\varepsilon}f(\phi_0)\Delta d\partial_t d + \frac{(1-|\nabla d|^2)}{\varepsilon}f'(\phi_0)\Psi'\Big(\frac{d(x,t)}{\sqrt{2}\varepsilon}\Big)\frac{\partial_t d}{\sqrt{2}\varepsilon}\mathrm{d}x + \int_{\partial\Omega\setminus\Gamma}\frac{2}{\varepsilon}f(\phi_0)\partial_n d\partial_t d\mathrm{d}s\\
&\quad + \int_\Gamma \frac{2}{\varepsilon}f(\phi_0)\partial_n d\partial_t d + g'(\phi_0)(1-\phi_0^2)\frac{\partial_t d}{\sqrt{2}\varepsilon}\mathrm{d}s\\
&= -\int_\Omega \frac{2}{\varepsilon}f(\phi_0)\Delta d\partial_t d\,\mathrm{d}x + \int_\Gamma \frac{2}{\varepsilon}f(\phi_0)(\partial_n d - \cos\theta_Y)\partial_t d\,\mathrm{d}s + \int_{\partial\Omega\setminus\Gamma}\frac{2}{\varepsilon}f(\phi_0)\partial_n d\partial_t d\mathrm{d}s\\
&\approx -\int_\Omega \frac{2}{\varepsilon}f(\phi_0)\Delta d\partial_t d\,\mathrm{d}x + \int_\Gamma \frac{2}{\varepsilon}f(\phi_0)(\partial_n d - \cos\theta_Y)\partial_t d\,\mathrm{d}s.
\end{aligned}$$

In the derivations, we have used integration by part in the second equation, and used the facts that $|\nabla d| = 1$, $g'(\phi_0) = -\frac{\sqrt{2}}{2}\cos\theta_Y(1-\phi_0^2)$ and $f(\phi_0) = \frac{(1-\phi_0^2)^2}{4}$ in the third equation. In the last equation, we ignore the integral term on $\partial\Omega\setminus\Gamma$, since $f(\phi_0)\approx f(-1) = 0$ on $\partial\Omega\setminus\Gamma$. This can be seen from the equation (18) when the liquid-vapor interface $\{x|\phi_0(x,t)=0\}$ is far from the boundary $\partial\Omega\setminus\Gamma$.

The Rayleighian is approximated by

$$\begin{aligned}
\mathcal{R} &= \Phi + \dot{\mathcal{E}}_\varepsilon\\
&\approx \frac{1}{\varepsilon^2}\int_\Omega f(\phi_0)\big((\partial_t d)^2 - 2\varepsilon\Delta d\partial_t d\big)\mathrm{d}x + \frac{1}{\varepsilon^2}\int_\Gamma f(\phi_0)(\xi\partial_t d + 2\varepsilon(\partial_n d - \cos\theta_Y))\partial_t d\,\mathrm{d}s.
\end{aligned}$$

It is easy to see that Fréchet derivative of $\mathcal{R}$ with respect to $\partial_t d$ is given by

$$\langle\frac{\delta\mathcal{R}}{\delta(\partial_t d)},\psi\rangle \approx \int_\Omega \frac{2}{\varepsilon^2}f(\phi_0)(\partial_t d - \varepsilon\Delta d)\psi\,\mathrm{d}x + \int_\Gamma \frac{2}{\varepsilon^2}f(\phi_0)(\xi\partial_t d + \varepsilon\partial_n d - \varepsilon\cos\theta_Y)\psi\,\mathrm{d}s$$

By using the Onsager principle, the dynamic equation for d is obtained by minimizing the approximated Rayleighian with respect to $\partial_t d$. This leads to a linear heat equation for d,

$$\begin{cases} \partial_t d - \varepsilon\Delta d = 0, & \text{in } \Omega;\\ \xi\partial_t d + \varepsilon(\partial_n d - \cos\theta_Y) = 0, & \text{on } \Gamma. \end{cases} \tag{22}$$

We can see that when $\xi = 0$, the condition on Γ is a standard Neumann boundary condition; and when $\xi > 0$, it is a linear dynamic boundary condition.

The equation (22) is much easier to solve than (17) since it is a linear equation with a linear boundary condition. However, the property $|\nabla d| = 1$ is not preserved by the solution of the heat equation (22). Therefore, $\tanh(\frac{d(x,t)}{\sqrt{2}\varepsilon})$ is a good approximation for the solution of (17) only when t is small. Nevertheless, it is enough for us to derive a numerical scheme if we re-distance the solution of (22) every time step.

4.2. The numerical scheme

We will construct a numerical method for the wetting problem (8). It includes the following three main steps: first to solve the linear diffusion equation (22), then to re-distance its solution, thirdly to correct the volume of the liquid domain. More details are described as follows.

Solving a heat equation. Given a signed distance function d_k, suppose that the liquid phase is given by $D_1^k = \{x : d_k(x) > 0\}$ and such that $|D_1^k| = V_0$. We first solve the following heat equation until time δt:

$$\begin{cases} \partial_t \varphi - \Delta \varphi = 0, & \text{in } \Omega; \\ \xi \partial_t \varphi + \partial_n \varphi = \cos\theta_Y, & \text{on } \Gamma; \\ \varphi(x,0) = d_k(x). \end{cases} \tag{23}$$

The equation is equivalent to (22) after a time scaling. In the above equation, we have not fixed the condition for φ on the boundary $\partial\Omega \setminus \Gamma$. Since we assume the boundary is far from the liquid-vapor interface, we could choose the boundary condition freely. For example, we can choose a Dirichlet boundary condition $\varphi = d_k(x)$ or a Neumann boundary condition $\partial_n \varphi = 0$. In our simulations, we simply set $\partial_n \varphi = 0$ on $\partial\Omega \setminus \Gamma$.

Since the equation (23) is a linear diffusion equation, many standard numerical methods can be used. In our simulations, we use the backward Euler scheme to discretize the time derivative that $\partial_t \varphi = \frac{\varphi^{n+1} - \varphi^n}{\delta t}$, where δt is the time step size. For the Laplace operator, we adopt the standard five point finite difference scheme to discretize it. Namely, for a uniform partition of $\Omega = (x_0, x_1) \times (y_0, y_1)$ with mesh size h, for the grid points inside Ω, we set

$$\frac{\varphi_{i,j}^{n+1} - \varphi_{i,j}^n}{\delta t} - \frac{\varphi_{i-1,j}^{n+1} + \varphi_{i+1,j}^{n+1} + \varphi_{i,j+1}^{n+1} + \varphi_{i,j-1}^{n+1} - 4\varphi_{i,j}^{n+1}}{h^2} = 0.$$

On the lower boundary Γ, we discretize a dynamic boundary condition as follows,

$$(1 + \frac{2\xi}{h})\frac{\varphi_{i,1}^{n+1} - \varphi_{i,1}^n}{\delta t} - \frac{\varphi_{i-1,1}^{n+1} + \varphi_{i+1,1}^{n+1} + 2\varphi_{i,2}^{n+1} - 4\varphi_{i,1}^{n+1}}{h^2} = \frac{2\cos\theta_Y}{h}.$$

It is a combination of the discretization of the linear diffusion equation and the discretization of dynamic relaxed boundary conditions. When $\xi = 0$, this equation is reduced to the standard finite difference discretization of the Neumann boundary condition.

For simplicity in notations, we denote the process of solving the heat equation (23) by

$$\varphi(x, \delta t) = \text{EquSolver}(d_k, \delta t).$$

The re-distance of the function φ. Since the solution $\varphi(x, \delta t)$ is not a signed distance function, we need to transform it into a signed distance function while keeping its zero level set unchanged. Denote by $\tilde{d}_{k+1}$ the signed distance function with respect to $\varphi(x, \delta t)$, satisfying

$$\nabla \tilde{d}_{k+1} = \frac{\nabla \varphi(x, \delta t)}{|\nabla \varphi(x, \delta t)|}$$

on the interface. Computing $\tilde{d}_{k+1}$ from $\varphi(x, \delta t)$ is the standard re-distance process in the level-set method. Many efficient algorithms have been developed(e.g. [54, 55, 56, 57, 58]). Here we adopt the method based on a fast marching technique [54]. We denote the re-distance process by

$$\tilde{d}_{k+1} = \text{Redist}(\varphi(x, \delta t)).$$

Correction of the volume. Finally, notice that the volume of the domain surrounded by the zero level-set of $\tilde{d}_{k+1}$ is not equal to the initial value V_0. To preserve the volume of the liquid domain, we need to make some correction for $\tilde{d}_{k+1}$ as in the volume-preserving threshold dynamics method [59]. We first search for a constant δ^* such that the domain $|\{x|\tilde{d}_{k+1}(x) > \delta^*\}| = V_0$, and then set

$$d_{k+1}(x) = \tilde{d}_{k+1}(x) - \delta^*.$$

Generally speaking, to find a constant δ^* efficiently is not easy[59, 26, 60]. In our numerical simulations, we use a simple bisection method. For that purpose, we must have an interval containing δ^*. For that purpose, we first find an estimate of δ^* using the method of counting the grid number as in [12]. Suppose we have a uniform partition for Ω with mesh size h. We sort the values $\tilde{d}_{k+1}(x_{ij})$ on the grid points into a decreasing array $\mathcal{S}$. Then δ^* can be approximated roughly by a value $\hat{\delta} = (\mathcal{S}(M) + \mathcal{S}(M+1))/2$, where $M = \lfloor V_0/h^2 \rfloor$, the integer part of V_0/h^2. We then easily extend it into a small interval which contains δ^*.

Repeat the above three steps iteratively. We get a series of signed distance function d_k, $k = 0, 1, \cdots$. Each d_k corresponds to a liquid domain D_1^k satisfying $|D_1^k| = V_0$. We expect that $\{D_1^k, D_2^k\}$ with $D_2^k := \Omega \setminus D_1^k$ gives an energy decreasing sequence for the problem (8). (The property will be studied in next section.) This leads to the following diffusion generated motion algorithm for the wetting problem.

Algorithm 1

Step 0. Give an initial signed distance function d_0 such that $|\{x|d_0(x) > 0\}| = V_0$, a constant tolerance TOL, and set $k = 0$.

Step 1. Solve the heat equation (23) with initial function d_k until a time δt (only one implicit Euler step) to obtain

$$\varphi(x, \delta t) = \text{EquSolver}(d_k, \delta t). \tag{24}$$

Step 2. Construct the signed distance function $\tilde{d}_{k+1}$ from $\varphi(x, \delta t)$

$$\tilde{d}_{k+1} = \text{Redist}(\varphi(x, \delta t)). \tag{25}$$

Step 3. Find a constant δ^* such that the domain $|\{x|\tilde{d}_k(x) > \delta^*\}| = V_0$. Set

$$d_{k+1}(x) = \tilde{d}_{k+1}(x) - \delta^*.$$

Step 4. If $\|d_{k+1} - d_k\| < TOL$, stop. Otherwise, set $k = k + 1$ and go back to **Step 1**.

The algorithm is much more efficient than directly solving the modified Allen-Cahn equation (16), since we avoid to resolve the very thin inner layer induced by a small parameter ε and also avoid the nonlinear boundary condition on Γ. Furthermore, there usually exist rough or chemically inhomogeneous boundaries in wetting problems. When we use the Allen-Cahn equation to simulate such problems, the interface thickness parameter ε must be chosen much smaller than the characteristic length of the microscopic roughness. This is extremely expensive in general. Notice that the parameter ξ in the dynamic boundary condition in (23) can be regarded as an adjustable parameter when we are only interested in the stationary state of wetting problems. Finally, if the boundary condition is replaced by a periodic boundary condition, the method is reduced to the standard method in [25] for mean curvature flows. Here the main difference is that we use a special boundary condition, which is used to describe the contact angle condition in wetting problems.

Remark 4.1. *In the above algorithm, we first do redistance and then correct the volume. This makes it convenient to do stability analysis by some geometric arguments as shown in next section. In applications, one may first correct the volume and then do redistance as in [25]. This leads to a slight different numerical scheme.*

5. Energy stability analysis

We study the energy stability property for Algorithm 1 in this section. As mentioned above, for any given d_0, which corresponds to a liquid domain $D_1^0 = \{x | d_0(x) > 0\}$, the algorithm generates a sequence of d_k. Each d_k corresponds to a liquid domain $D_1^k = \{x | d_k(x) > 0\}$. This implies that Algorithm 1 generates a (discrete) evolution of a liquid domain. We will prove the total wetting energy (7) corresponding to the liquid domain D_1^k(by setting $D_2^k = \Omega \setminus D_1^k$) decays when k increases. For that purpose, we will first reformulate the main processes in Algorithm 1 into some geometric flows for the surface of the liquid domain. Then we will prove some energy decay property for the geometric flows. Hereinafter we restrict our analysis in two dimensions. For simplicity, we assume the liquid domain D_1^k is simply connected.

5.1. The approximate geometric flows for Algorithm 1

We first consider Step 1 in Algorithm 1. When δt is small , the zero level set of the solution of the linear diffusion equation (23) approximates a mean curvature flow problem starting from a curve $\{x \in \Omega \,|\, d_k(x) = 0\}$ with the contact angle being given by Young's angle θ_Y. Here a mean curvature flow denotes a geometric flow for a curve which evolves with the normal velocity equal to its local (mean) curvature. When the zero level set of φ has no intersection with the solid boundary Γ, the relation between the solution of the heat equation and the mean curvature flow has been shown in [25]. The approximation error is of order $O(\delta t^2)$(c.f. Equation (66)-(67) in [25]). The analysis still works for (23) for the inner points on the zero level set of $\varphi(x,t)$. We need only to study the contact angle condition. On the zero level set of $\varphi(x,t)$, its normal direction is given by $\frac{\nabla\varphi}{|\nabla\varphi|}$. The contact angle θ between the zero level set of $\varphi(x,t)$ and the solid boundary Γ satisfies

$$\cos\theta = \frac{\nabla\varphi}{|\nabla\varphi|}\cdot\mathbf{n} = \frac{1}{|\nabla\varphi|}\partial_n\varphi.$$

We consider motion of the zero level set of φ. Suppose $X(t)$ is a point on the zero level set. We have $\varphi(X,t)\equiv 0$. Then we have $0 = \frac{d\varphi}{dt} = \partial_t\varphi + \nabla\varphi\cdot\frac{dX}{dt}$. This leads to

$$\partial_t\varphi = -|\nabla\varphi| v_N,$$

where $v_N = \frac{dX}{dt}\cdot\frac{\nabla\varphi}{|\nabla\varphi|}$ is the velocity normal to the zero level set of φ. By the above two equations, we can see that the boundary condition of (23) is reduced to

$$-\xi|\nabla\varphi| v_N + |\nabla\varphi|\cos\theta = \cos\theta_Y. \tag{26}$$

Suppose the two contact points of the zero level set of φ on the substrate are respectively X_0(the right one) and X_1(the left one), and the corresponding contact angles are θ_0 and θ_1. The horizontal velocity of the two contact points on the substrate are v_0 and v_1. We have $v_N(X_0) = -v_0\sin\theta_0$ and $v_N(X_1) = v_1\sin\theta_1$. Then the above equation (26) is reduced to

$$\xi v_0 = (\cos\theta_Y/|\nabla\varphi| - \cos\theta_0)/\sin\theta_0, \qquad \xi v_1 = (\cos\theta_1 - \cos\theta_Y/|\nabla\varphi|)/\sin\theta_1. \tag{27}$$

The analysis(c.f. Equation (30) in [25]) shows that

$$|\nabla\varphi(x,\delta t)| \approx |\nabla\varphi(x,0)| + O(\delta t) = 1 + O(\delta t),$$

in the vicinity of the zero level set of φ. Therefore (27) implies that

$$\xi v_0 \approx (\cos\theta_Y - \cos\theta_0)/\sin\theta_0, \qquad \xi v_1 \approx (\cos\theta_1 - \cos\theta_Y)/\sin\theta_1. \tag{28}$$

In all, Step 1 of Algorithm 1 leads to a mean curvature flow for the surface of the liquid domain with the contact point velocity given by Equation (28).

For Step 2 in Algorithm 1, i.e. the re-distance step, the zero level-set of $\tilde{d}_{k+1}$ is the same as that for $\varphi(x,\delta t)$. This implies the liquid domain is unchanged in this step. Then we need only further consider

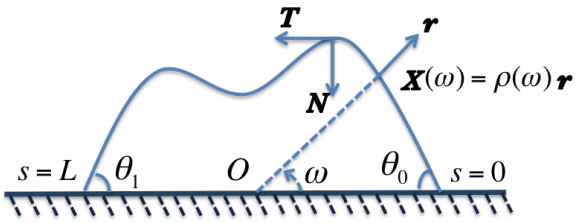

Figure 2: The evolving curve with constraints

Step 3 (the volume correction step) in Algorithm 1. Since $\tilde{d}_{k+1}$ is a signed distance function, it is easy to see that the volume correction step corresponds to a motion of the zero level-set of $\tilde{d}_{k+1}$ with a constant normal velocity. More precisely, the zero level-set of d_{k+1} is obtained by moving the zero level-set of $\tilde{d}_{k+1}$ in a constant normal velocity equal to -1 until a time δ^*.

By the above analysis, one iteration of Algorithm 1 can be approximated by two geometric flows (a mean curvature flow and a constant normal velocity flow) for the surface of a liquid domain. For convenience in later analysis, we characterize the two geometric flows more precisely as follows.

- **Process 1.** At $t = t_0 = 0$, d_k gives a droplet with a free boundary curve $\mathcal{L}_0$(as shown in Figure 2). The boundary $\mathcal{L}(t) := \{\boldsymbol{X}(s,t) : 0 \le s \le L(t)\}$ of the droplet evolves under a mean curvature flow in the sense that $v_n = \kappa$ and the boundary condition (28). Here s is the arc-length parameter, $L(t)$ is the length of the curve $\mathcal{L}(t)$ at time t, and θ_i with $i = 0, 1$ are the contact angles at the two ends of $\mathcal{L}(t)$. This process ends until $t_1 = t_0 + \delta t$ and then we denote $\mathcal{L}_1 = \mathcal{L}(t_1)$. In this process, the volume of the droplet is denoted by $A(t)$ which decreases with time. We set $A_0 = A(t_0) = V_0$ and $A_1 = A(t_1)$.

- **Process 2.** Starting from $\mathcal{L}_1$ at $t = t_1$, the boundary $\hat{\mathcal{L}}(t) := \{\hat{\boldsymbol{X}}(s,t) : 0 < s < \hat{L}(t)\}$ of the droplet moves under a constant velocity flow with $v_n = -1$. Here s is the arc-length parameter and $\hat{L}(t)$ is the length of the curve $\hat{\mathcal{L}}(t)$ at time t. Notice that we have set $\hat{\mathcal{L}}(t_1) = \mathcal{L}_1$. If we denote the volume of the droplet as $A(t)$ in the process, it is an increasing function with respect to time t such that $A(t_1) = A_1$. The process ends until $t_2 = t_1 + \delta^*$ such that the liquid volume corresponding to $\hat{\mathcal{L}}(t_2)$ is equal to that to $\mathcal{L}_0$, namely $A(t_2) = A_0 = V_0$.

Here we use different notations $\mathcal{L}$ and $\hat{\mathcal{L}}$ for the curve of a droplet in the two different processes. We will show the total energy decreases after an iteration of Process 1 and Process 2.

5.2. Energy decay property for the geometric flows

In the following, we will analyse the energy decay property of an iteration of Process 1 and Process 2. This is based on a careful analysis of the properties of the corresponding geometric flows in the two processes. We first introduce some results for a general geometric flow for a curve with both ends on a substrate.

As shown in Figure 2, we consider a smooth curve on a substrate, which represents the surface of a liquid droplet. The liquid domain is simply connected so that the curve does not intersect itself. For simplicity, we assume the curve can be represented by a function in a polar coordinate as $\{\boldsymbol{X}(\omega) : 0 \le \omega \le \pi\}$. The curve evolves with time and can be noted by $\{\boldsymbol{X}(\omega, t)\}$. Its length is given by $L(t)$. Notice that the curve can also be represented in an arclength parameter s that $\{\boldsymbol{X}(s,t) : 0 \le s \le L(t)\}$. Then we have $\boldsymbol{T} = \partial_s \boldsymbol{X}$ and $\partial_s \boldsymbol{T} = \kappa \boldsymbol{N}$. Here $\boldsymbol{N}$ and $\boldsymbol{T}$ are respectively the unit normal vector and the unit tangential vector on the curve. $\boldsymbol{N}$ is obtained by rotating $\boldsymbol{T}$ for 90^o in the counter-clockwise direction. $\kappa(s)$ is the curvature of the curve, which is positive when the center of the circle of curvature is in the same direction of $\boldsymbol{N}$. In addition, we have the relation that $\partial_\omega \boldsymbol{X} = |\partial_\omega \boldsymbol{X}| \boldsymbol{T}$ and $\mathrm{d}\omega = |\partial_\omega \boldsymbol{X}| \mathrm{d}s$. Here $|\cdot|$ is the norm of a vector in $\mathbb{R}^2$.

We use v_n and v_s to represent the radial and tangential components of velocity respectively. Then the velocity can be written as

$$\boldsymbol{X}_t = \boldsymbol{v} = \boldsymbol{v}_n + \boldsymbol{v}_s = v_n \boldsymbol{N} + v_s \boldsymbol{T}.$$

We are interested in how the length of the curve and the area of the liquid domain (enclosed by the curve and substrate) change when the curve evolves with time. This is given by the following lemma, which is adapted from the result for closed curves(see Section 3.2 in [61]).

Lemma 5.1. *For an evolving curve as shown Figure 2, let $L(t)$ be the length of the curve, and $A(t)$ be the area enclosed by the curve and the lower substrate. Then, we have*

$$\frac{\mathrm{d}L(t)}{\mathrm{d}t} = -\int_0^L \kappa v_n \mathrm{d}s + v_x(0)\cos\theta_0 - v_x(L)\cos\theta_1, \tag{29}$$

$$\frac{\mathrm{d}A(t)}{\mathrm{d}t} = -\int_0^L v_n \mathrm{d}s. \tag{30}$$

where θ_0 and θ_1 are respectively the contact angles at the points corresponding to $s = 0$ and $s = L(t)$; $v_x(0)$ and $v_x(L)$ are respectively the velocities of the two end points in x direction.

Proof. For proof of (29) we argue as follows. Here we use $\langle\cdot,\cdot\rangle$ to donate inner product of the vector in $\mathbb{R}^2$.

$$\begin{aligned}
\frac{\mathrm{d}}{\mathrm{d}t}L(t) &= \frac{\mathrm{d}}{\mathrm{d}t}\int_0^\pi \langle\partial_\omega \boldsymbol{X}, \partial_\omega \boldsymbol{X}\rangle^{1/2}\,\mathrm{d}\omega = \int_0^\pi \frac{\langle\partial_{t\omega}\boldsymbol{X}, \partial_\omega \boldsymbol{X}\rangle}{\langle\partial_\omega \boldsymbol{X}, \partial_\omega \boldsymbol{X}\rangle^{1/2}}\mathrm{d}\omega \\
&= \int_0^\pi \left\langle \frac{\partial}{\partial\omega}(v_n\boldsymbol{N} + v_s\boldsymbol{T}), \boldsymbol{T}\right\rangle \mathrm{d}\omega = \int_0^\pi \left\langle |\partial_\omega \boldsymbol{X}|\,\frac{\partial}{\partial s}(v_n\boldsymbol{N} + v_s\boldsymbol{T}), \boldsymbol{T}\right\rangle \mathrm{d}\omega \\
&= \int_0^{L(t)} \left\langle \frac{\partial}{\partial s}(v_n\boldsymbol{N} + v_s\boldsymbol{T}), \boldsymbol{T}\right\rangle \mathrm{d}s \\
&= -\int_0^{L(t)} v_n\kappa \mathrm{d}s + \int_0^{L(t)} \partial_s v_s \mathrm{d}s = -\int_0^{L(t)} v_n\kappa \mathrm{d}s + v_s(L) - v_s(0).
\end{aligned}$$

In the last second derivation, we have used the geometric equation that $\partial_s \boldsymbol{N} = -\kappa\boldsymbol{T}$. Since the two end points can only move in horizontal direction, we have the constraint

$$v_s(L) = -v_x(L)\cos\theta_1, \qquad v_s(0) = -v_x(0)\cos\theta_0. \tag{31}$$

Then we have proved the equation (29).

The proof of (30) can be done as follows. Notice that the curve can also be written as $\boldsymbol{X}(\omega, t) = \rho(\omega, t)\boldsymbol{r}(\omega)$, where $\boldsymbol{r}(\omega)$ is the unit vector in the radial direction. Then we have

$$\partial_\omega \boldsymbol{X}(\omega, t) = \partial_\omega \rho(\omega, t)\boldsymbol{r}(\omega) + \rho(\omega, t)\vec{\theta}(\omega),$$

where $\vec{\theta}(\omega)$ is the unit vector in the angular direction. Then we have

$$\partial_{t\omega} \boldsymbol{X}(\omega, t) = \partial_{t\omega} \rho(\omega, t)\boldsymbol{r}(\omega) + \partial_t \rho(\omega, t)\vec{\theta}(\omega).$$

We define an outer product for vectors $\boldsymbol{a} = (a_1, a_2)^T, \boldsymbol{b} = (b_1, b_2)^T \in \mathbb{R}^2$ (see Page 22 in [61]) as

$$[\boldsymbol{a}, \boldsymbol{b}] := \det\begin{pmatrix} a_1 & b_1 \\ a_2 & b_2 \end{pmatrix} = a_1 b_2 - a_2 b_1,$$

which is a bilinear operator for the two vectors. This leads to

$$[\boldsymbol{X}(\omega, t), \partial_{t\omega}\boldsymbol{X}(\omega, t)] = \rho(\omega, t)\partial_t \rho(\omega, t)\left[\boldsymbol{r}(\omega), \vec{\theta}(\omega)\right] = \rho(\omega, t)\partial_t \rho(\omega, t).$$

Then we have

$$\begin{aligned}\frac{\mathrm{d}}{\mathrm{d}t}A(t) &= \frac{\mathrm{d}}{\mathrm{d}t}\int_0^\pi \frac{1}{2}(\rho(\omega,t))^2\mathrm{d}\omega = \int_0^\pi \rho(\omega,t)\partial_t\rho(\omega,t)\mathrm{d}\omega\\ &= \int_0^\pi [\boldsymbol{X}(\omega,t),\partial_{t\omega}\boldsymbol{X}(\omega,t)]\,\mathrm{d}\omega = \int_0^\pi [\boldsymbol{X}(\omega,t),\partial_\omega\boldsymbol{v}(\omega,t)]\,\mathrm{d}\omega\\ &= [\boldsymbol{X}(\omega,t),\boldsymbol{v}(\omega,t)]\,|_0^\pi - \int_0^\pi [\partial_\omega\boldsymbol{X}(\omega,t),\boldsymbol{v}(\omega,t)]\,\mathrm{d}\omega\\ &= -\int_0^\pi [|\partial_\omega\boldsymbol{X}|\boldsymbol{T},\boldsymbol{v}(\omega,t)]\,\mathrm{d}\omega = -\int_0^{L(t)} [\boldsymbol{T},\boldsymbol{v}(\omega,t)]\,\mathrm{d}s\\ &= -\int_0^{L(t)} v_n\mathrm{d}s.\end{aligned}$$

In the derivation, we have used the integration by part, the fact that all the vectors $\boldsymbol{v}(0)$, $\boldsymbol{v}(\pi)$, $\boldsymbol{X}(0)$ and $\boldsymbol{X}(\pi)$ are in the horizontal direction, $[\boldsymbol{T},\boldsymbol{T}]=0$ and $[\boldsymbol{T},\boldsymbol{N}]=1$. We finish the proof of the lemma. □

In wetting problems, we mainly interested in the total surface energy in a liquid-vapor-solid system, which is defined in (7). For a droplet as in Figure 2, the wetting energy can be rewritten as

$$\mathcal{E}(t) = \gamma\left(L(t) - |\boldsymbol{X}(0)-\boldsymbol{X}(L)|\cos\theta_Y\right) + C.$$

Here $\gamma=\gamma_{LV}$ and $C = C_0 + \frac{\gamma}{2}|\Gamma|\cos\theta_Y$. Here we assume that the contact angle θ_Y is a constant on the solid surface Γ. Applying Lemma 5.1 directly yields,

Lemma 5.2. *For a droplet with an evolving surface as shown in Figure 2, the total wetting energy satisfies*

$$\frac{\mathrm{d}\mathcal{E}(t)}{\mathrm{d}t} = -\gamma\int_0^{L(t)} \kappa v_n\mathrm{d}s + \gamma v_0(\cos\theta_0-\cos\theta_Y) - \gamma v_1(\cos\theta_1-\cos\theta_Y), \tag{32}$$

Proof. Apply Lemma 5.1 directly to get

$$\begin{aligned}\frac{\mathrm{d}}{\mathrm{d}t}L(t) - \frac{\mathrm{d}}{\mathrm{d}t}|\boldsymbol{X}(0)-\boldsymbol{X}(L)|\cos\theta_Y &= \left(-\int_0^L \kappa v_n\mathrm{d}s + v_0\cos\theta_0 - v_1\cos\theta_1\right) - (v_0-v_1)\cos\theta_Y\\ &= -\int_0^L \kappa v_n\mathrm{d}s + v_0(\cos\theta_0-\cos\theta_Y) - v_1(\cos\theta_1-\cos\theta_Y).\end{aligned}$$

□

Gathering the results above readily gives the following properties for the geometric flows in Process 1 and Process 2 defined in Section 5.1.

Proposition 5.1. *For the geometric flow in Process 1, in which the normal velocity is equal to the mean curvature($v_n=\kappa$) and the contact angle is determined by (28), we have*

$$\frac{\mathrm{d}\mathcal{E}}{\mathrm{d}t} = -\gamma\int_0^{L(t)} \kappa^2\mathrm{d}s - \gamma\xi^{-1}\frac{(\cos\theta_0-\cos\theta_Y)^2}{\sin\theta_0} - \gamma\xi^{-1}\frac{(\cos\theta_1-\cos\theta_Y)^2}{\sin\theta_1}, \tag{33}$$

$$\frac{\mathrm{d}A}{\mathrm{d}t} = -(\theta_0+\theta_1). \tag{34}$$

For the geometric flow in Process 2, in which the normal velocity is a constant($v_n=-1$), then we have

$$\frac{\mathrm{d}\mathcal{E}}{\mathrm{d}t} = \gamma(\theta_0+\theta_1) + \gamma\frac{(\cos\theta_0-\cos\theta_Y)}{\sin\theta_0} + \gamma\frac{(\cos\theta_1-\cos\theta_Y)}{\sin\theta_1}, \tag{35}$$

$$\frac{\mathrm{d}A}{\mathrm{d}t} = \hat{L}(t). \tag{36}$$

Proof. The proposition is directly obtained from the previous two lemmas. We first consider Process 1. Equation (33) comes from (32) by noticing $v_n = \kappa$ and the boundary condition (28). To show Equation (34), we need to use (30) and the standard local Gauss-Bonnet theorem for closed planar curves [62] that

$$\int_0^L \kappa \mathrm{d}s + 0 \cdot |X(0) - X(L)| + (\pi - \theta_0) + (\pi - \theta_1) = 2\pi.$$

This simply gives $\int_0^L \kappa \mathrm{d}s = \theta_0 + \theta_1$. For Process 2, the results can be proved similarly noticing that the normal velocity is $v_n = -1$ and the contact point velocities are $v_0 = -v_n/\sin\theta_0$ and $v_1 = v_n/\sin\theta_1$. □

The proposition implies that the total energy decays in Process 1 while it might increase in Process 2. In the following, we study the energy decay property of an iteration of Process 1 and Process 2. We will focus on the case where the local contact angles are equal to the Young's angle. This holds when $\xi = 0$ in (28) or approximately holds in the final states when ξ is small. For clarity in presentation, we introduce a few more notations. Let $A_0 = A(t_0)$, $A_1 = A(t_1)$ and $A_2 = A(t_2)$ be the volumes(areas) of the droplet at the beginning of Process 1, at the end of Process 1(or equivalently the beginning of Process 2) and the end of Process 2, respectively. Similarly, $\mathcal{E}_i, i = 0, 1, 2$ are respectively the total wetting energies in the corresponding states.

Theorem 5.1. *For a droplet as shown in Figure 2, it evolves by a mean curvature flow as described in Process 1 in the first stage ($t_0 < t < t_1$), and then correct its volume to initial value A_0 by a constant velocity flow as described in Process 2 in the second stage ($t_1 < t < t_2$). If we assume that $\mathcal{L}(t_1)$ is not a circular curve and $\theta_0 = \theta_1 = \theta_Y$ holds in the two processes, then the total wetting energy decreases after an iteration of Process 1 and Process 2, namely*

$$\mathcal{E}_2 \leq \mathcal{E}_0. \tag{37}$$

when δt is small enough.

Proof. By Lemma 5.1, we obtain the relation of the wetting energies,

$$\mathcal{E}_0 - \mathcal{E}_1 = \gamma \int_{t_0}^{t_1} \int_0^{L(t)} \kappa^2 \mathrm{d}s\mathrm{d}t = \gamma \int_{t_1 - \delta t}^{t_1} \int_0^{L(t)} \kappa^2 \mathrm{d}s\mathrm{d}t =: I, \tag{38}$$

$$\mathcal{E}_2 - \mathcal{E}_1 = 2\gamma\theta_Y(t_2 - t_1) = 2\gamma\theta_Y\delta^* =: II. \tag{39}$$

We need only to prove

$$II \leq I. \tag{40}$$

For the volume of the droplet, we have

$$A_0 - A_1 = 2\theta_Y \delta t, \tag{41}$$

$$A_2 - A_1 = \int_{t_1}^{t_2} \hat{L}(t)\mathrm{d}t. \tag{42}$$

From the proof of Lemma 2, we know that, for the constant velocity flow in Process 2,

$$\frac{d\hat{L}(t)}{dt} = 2\theta_Y + (v_x(0) - v_x(\hat{L}))\cos\theta_Y. \tag{43}$$

Notice that $v_x(0)\sin\theta_Y = -v_n = 1$ and $v_x(L)\sin\theta_Y = v_n = -1$. So we have $\frac{d\hat{L}(t)}{dt} = 2(\theta_Y + \operatorname{ctan}\theta_Y)$. This leads to $\hat{L}(t) - \hat{L}(t_1) = 2(\theta_Y + \operatorname{ctan}\theta_Y)(t - t_1)$. Then the right hand side term of the equation (42) can be computed as

$$\int_{t_1}^{t_2} \hat{L}(t)\mathrm{d}t = \delta^*\big(\hat{L}(t_1) + (\theta_Y + \operatorname{ctan}\theta_Y)\delta^*\big).$$

Due to the volume correction condition that $A_0 = A_2$, we have

$$2\theta_Y \delta t = \delta^* \big(\hat{L}(t_1) + (\theta_Y + \operatorname{ctan}\theta_Y)\delta^*\big). \tag{44}$$

This leads to $\delta^* = \frac{\sqrt{\hat{L}(t_1)^2 + 8\theta_Y(\theta_Y + \operatorname{ctan}\theta_Y)\delta t} - \hat{L}(t_1)}{2(\theta_Y + \operatorname{ctan}\theta_Y)}$. Notice that $\hat{L}(t_1)$ is the same as $L(t_1)$. We have

$$\delta^* = \frac{\sqrt{L(t_1)^2 + 8\theta_Y(\theta_Y + \operatorname{ctan}\theta_Y)\delta t} - L(t_1)}{2(\theta_Y + \operatorname{ctan}\theta_Y)}. \tag{45}$$

Then we have

$$\begin{aligned} II = 2\gamma\theta_Y\delta^* &= \frac{\gamma\theta_Y}{\theta_Y + \operatorname{ctan}\theta_Y}\big(\sqrt{L(t_1)^2 + 8\theta_Y(\theta_Y + \operatorname{ctan}\theta_Y)\delta t} - L(t_1)\big) \\ &= \gamma \int_{t_1}^{t_1+\delta t} \frac{4\theta_Y^2}{\sqrt{L(t_1)^2 + 8\theta_Y(\theta_Y + \operatorname{ctan}\theta_Y)(t - t_1)}} \mathrm{d}t \\ &= \gamma \int_{t_1-\delta t}^{t_1} \frac{4\theta_Y^2}{\sqrt{L(t_1)^2 + 8\theta_Y(\theta_Y + \operatorname{ctan}\theta_Y)(t_1 - t)}} \mathrm{d}t =: \gamma \int_{t_1-\delta t}^{t_1} \tilde{g}(t)\mathrm{d}t \end{aligned} \tag{46}$$

It is easy to see that

$$\tilde{g}(t_1) = \frac{4\theta_Y^2}{L(t_1)}.$$

By Cauchy-Buniakowsky-Schwarz inequality, we have

$$2\theta_Y = \int_0^{L(t_1)} \kappa \mathrm{d}s \le \Big(\int_0^{L(t_1)} \kappa^2 \mathrm{d}s\Big)^{1/2} (L(t_1))^{1/2}.$$

The equality holds only when κ is a constant on $\mathcal{L}(t_1)$. This implies

$$\tilde{g}(t_1) < \int_0^{L(t_1)} \kappa^2 \mathrm{d}s. \tag{47}$$

when $\mathcal{L}(t_1)$ is not a circular curve. Since $\tilde{g}(t)$ is a smooth function with respect to t, we then have

$$\int_{t_1-\delta t}^{t_1} \tilde{g}(t)dt \le \int_{t_1-\delta t}^{t_1} \int_0^{L(t)} \kappa^2 \mathrm{d}s. \tag{48}$$

when δt is small enough. This ends the proof of the theorem. □

To show the unconditional energy decay property of the geometric flows by Process 1 and Process 2, we need a nice geometric estimate for the elastic energy

$$E(\gamma) = \frac{1}{2}\int_\gamma \kappa^2 ds$$

for a curve γ under some constraints for the enclosed area. The needed inequality is sharper than the standard isoperimetric inequalities [65, 66] and has been proved only recently for closed smooth curves [63, 64]. We can apply them for the wetting problem only when $\theta_Y = \frac{\pi}{2}$. We first show the following lemma which is a direct generalization of the results in [63, 64].

Lemma 5.3. *For any simple regular curve $\gamma \in W^{2,2}$ in $\mathbb{R}^2$ which has a contact angle $\theta_Y = \frac{\pi}{2}$ with the substrate, we denote by $A(\gamma)$ the area enclosed by the curve and the substrate, and by $E(\gamma) = \frac{1}{2}\int_\gamma \kappa(s)^2 ds$ the elastic energy, then we have*

$$A(\gamma)E(\gamma)^2 \ge \frac{\pi^3}{8}, \tag{49}$$

and the equality holds if and only if γ is a circular curve.

Proof. Since $\theta_Y = \frac{\pi}{2}$, one can construct a regular closed curve by reflection. Then the lemma is a direct consequence of Theorem 1 in [63] and Theorem 1.1 in [64], where it is proved that the inequality

$$A(\tilde{\gamma})E(\tilde{\gamma})^2 \geq \pi^3,$$

for any closed curve $\tilde{\gamma}$ and the equality holds only for a circle. Since both the area and the elastic energy in (49) are half of that for the corresponding closed curve, the inequality is derived directly. □

By this lemma, we can prove an unconditionally energy decay property for the geometric flows in an iteration of Process 1 and Process 2 when $\theta_Y = \frac{\pi}{2}$. More general cases will be discussed in the Appendix.

Proposition 5.2. *Under the condition of Theorem 5.1, when $\theta_Y = \frac{\pi}{2}$, we have*

$$\mathcal{E}_2 \leq \mathcal{E}_0. \tag{50}$$

for any $\delta t > 0$ such that $L(t_1) > 0$.

Proof. As shown in the calculations in Theorem 5.1(see (38) and (46)), we need only prove

$$\tilde{g}(t) \leq \int_0^{L(t)} \kappa^2 ds$$

for $t_1 - \delta t \leq t \leq t_1$. When $\theta_Y = \frac{\pi}{2}$, we have

$$\tilde{g}(t) = \frac{\pi^2}{\sqrt{L^2(t_1) + 2\pi^2(t_1 - t)}}.$$

We consider an auxiliary mean curvature flow for a half circle. The radius $\tilde{R}$ of the half circle satisfies that

$$\frac{d\tilde{R}}{dt} = -\frac{1}{\tilde{R}}.$$

Then the arc length $\tilde{L} = \pi\tilde{R}$ of the half circle satisfies

$$\frac{d\tilde{L}}{dt} = -\frac{\pi^2}{\tilde{L}}.$$

Suppose that $\tilde{L}(t_1) = L(t_1)$, we can easily see that the solution of the above equation is exactly $\tilde{L}(t) = \sqrt{L^2(t_1) + 2\pi^2(t_1 - t)}$. Then we have

$$\tilde{g}(t) = \frac{\pi^2}{\tilde{L}(t)} = \frac{\pi}{\tilde{R}} = \int_0^{\tilde{L}(t)} \tilde{\kappa}(t)^2 ds,$$

where $\tilde{\kappa} = \frac{1}{\tilde{R}}$ being the curvature of the half circle.

Now we need only compare the elastic energies for the curves in the mean curvature flow in Process 1 and the auxiliary mean curvature flow for the half circle. At time t_1, the two curves have the same arc length that $\tilde{L}(t_1) = L(t_1)$. Then we know that the half circle encloses larger area that $\tilde{A}(t_1) \geq A(t_1)$ by the standard isoperimetric inequality for droplets with contact angle $\frac{\pi}{2}$(see e.g. in [11]). Here we denote by $\tilde{A}(t)$ and $A(t)$ respectively the areas of the droplets corresponding to the half circle and the curve in Process 1. Notice that the area changes in the same rate of $-\pi$ in the two mean curvature flows by (34). We know that $\tilde{A}(t) \geq A(t)$ for all $t \in [t_1 - \delta t, t_1]$. We further consider a half circle $\check{\gamma}$ with a smaller radius $\check{R}(t)$ such that $\check{R}(t) \leq \tilde{R}(t)$ and $A(t) = \frac{\pi\check{R}^2}{2}$. Then we easily know that

$$\tilde{g}(t) = \frac{\pi}{\tilde{R}(t)} \leq \frac{\pi}{\check{R}(t)} = \int_{\check{\gamma}} \check{\kappa}^2 ds.$$

By Lemma 5.3, we know that

$$A(t)(\int_0^{L(t)} \kappa^2 ds)^2 = 4A(t)E(t)^2 \geq \frac{\pi^3}{2} = A(t)(\frac{\pi}{\check{R}(t)})^2.$$

The above two inequalities lead to

$$\int_0^{L(t)} \kappa^2 ds \geq \frac{\pi}{\check{R}(t)} \geq \tilde{g}(t).$$

This completes the proof of the proposition. □

Remark 5.1. *In Proposition 5.2, we show the unconditional stability result only for the case $\theta_Y = \frac{\pi}{2}$. For general cases, the analysis is much more complicated. In the appendix, we give some further discussions on the cases that $\theta_Y \neq \frac{\pi}{2}$. We can prove the energy decay property for large time step under some further assumptions. In addition, we would like to remark that the analysis in this paper is only for some approximated geometric flows for the algorithm in the Section 4. This is different from the analysis in [12, 13], where the unconditional stability is proved rigorously for the original threshold dynamics method.*

Remark 5.2. *Finally, it is very complicated to prove the stability results when θ_0 and θ_1 may change with time when $\xi \neq 0$. However, from Proposition 5.1, we can see that the energy decay property of Process 1 is enhanced when ξ is small. If we assume that the two contact angles θ_0 and θ_1 change very slowly so that they can be regarded as constants approximately in the two processes, one may estimate the energy decay behavior of the two processes when the time step δt and ξ are small. In addition, although we consider only flat substrates for simplicity in presentation, the analysis can be generalized to the case with curved boundaries. We will leave these for future work.*

6. Numerical examples

6.1. Accuracy check

In this subsection, we will show some numerical experiments to test the convergence rate with respect to δt for the diffusion generated motion method(Algorithm 1). For that purpose, we consider a liquid drop on a homogeneous planar surface. It is known that the problem (8) has an explicit solution. It corresponds to a circular droplet with the contact angle equal to Young's angle on the substrate. Therefore we can compute the stationary profile of a liquid drop for various Young's angles.

We first do tests for several choices of Young's angle θ_Y when $\xi = 0$. In all these tests, we set $\Omega = [0,1]^2$. We put the initial curve in the middle of the lower boundary of Ω. When Young's angle θ_Y is not equal to $90°$,we set the surface of the initial droplet as a semicircle with the radius $R_0 = 0.25$. When $\theta_Y = 90°$, the initial droplet is a circular domain with an initial volume $V_0 = \pi/16$ and with two contact points given by $(3/8, 0)$ and $(5/8, 0)$. We set $TOL = 10^{-10}$ in the algorithm. We find that Algorithm 1 always converges in the sense that the tolerance is obtained after some iterations. In each experiment, we use a uniform $N \times N$ mesh and fix a time step δt(as listed in Table 1-4), where we set a unit time as $t_{unit} = 1/64$. We compute the error in the following way,

$$Err_\infty := \text{dist}(\mathcal{L}_k, \mathcal{L}) = \sup_{\mathrm{x} \in \mathcal{L}_k} \inf_{\mathrm{y} \in \mathcal{L}} \|\mathrm{x} - \mathrm{y}\|$$

Here $\mathcal{L}_k$ represents the zero level set of the numerical solution d_k, $\mathcal{L}$ is the circular curve corresponding to the exact solution.

Figure 3 shows numerical solutions and the corresponding analytical solutions for the cases of $\theta_Y = 70^o, N = 32$ (left) and $\theta_Y = 110^o, N = 32$(right). We can see that our algorithm gives accurate results in both cases even on a relatively coarse mesh. More results on numerical errors are shown in Tables 1-4. We decrease the spacial mesh size and time step size proportionally. We can see that the error is of order

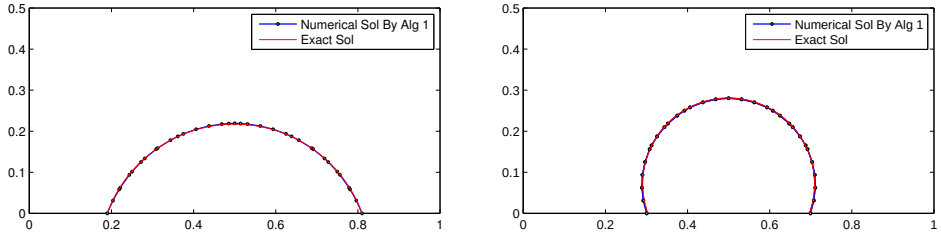

(a)$\theta = 70^o, N = 32$. (b)$\theta = 110^o, N = 32$.

Figure 3: A comparison between the numerical solution obtained by Algorithm 1 and the exact solution.

$O(\delta t)$ when $\theta_Y = 110^o, 100^o$ and 70^o. This is optimal as in the standard diffusion generated method for smooth curves[25]. When $\theta_Y = 90^o$, the convergence order is much better. This might be due to the error for time discretization is less dominant in this case, so that the error is of order $O(\delta x^2)$. In all, the diffusion generated motion method gives optimal convergence rate $O(\delta t)$ with respect to the time step for the wetting problems. This is better than the threshold dynamics method developed in [12, 13], where the convergence order is of $O(\delta t^{1/2})$, due to the existence of the contact points.

Table 1: Numerical errors of Algorithm 1 for the case $\theta_Y = 110$ °

# Resolution	# $\delta t(t_{unit})$	# Error	# Order
8×8	1/2	9.96E-3	-
16×16	1/4	5.31E-3	0.91
32×32	1/8	2.68E-3	0.99
64×64	1/16	1.67E-3	0.68
128×128	1/32	7.42E-4	1.17

Table 2: Numerical errors of Algorithm 1 for the case $\theta_Y = 100$ °

# Resolution	# $\delta t(t_{unit})$	# Error	# Order
8×8	1/2	1.42E-2	-
16×16	1/4	6.03E-3	1.24
32×32	1/8	2.26E-3	1.42
64×64	1/16	1.04E-3	1.12
128×128	1/32	4.58E-4	1.18

Table 3: Numerical errors of Algorithm 1 for the case $\theta_Y = 90$ °

# Resolution	# $\delta t(t_{unit})$	# Error	# Order
8×8	1/2	2.39E-2	-
16×16	1/4	6.17E-3	1.95
32×32	1/8	1.65E-3	1.90
64×64	1/16	3.59E-4	2.20
128×128	1/32	6.59E-5	2.44

We then give some numerical examples to illustrate the influence of the dynamic boundary condition when $\xi \neq 0$. We set $\theta_Y = \pi/3$. The numerical results are shown in Table 5 for different choices of ξ. It seems that the error increases slightly as the value of ξ increases while the convergence rate is almost of the same

Table 4: Numerical errors of Algorithm 1 for the case $\theta_Y = 70\ ^\circ$

# Resolution	# $\delta t(t_{unit})$	# Error	# Order
8×8	1	2.86E-2	-
16×16	1/2	1.09E-2	1.39
32×32	1/4	4.13E-3	1.40
64×64	1/8	1.12E-3	1.99
128×128	1/16	5.92E-4	0.92

order $O(\delta t)$. In many applications, since we are mainly interested in the stationary state or quasi-static processes of a liquid droplet on solid surfaces, we can choose ξ to be zero or a very small number.

Table 5: The numerical results using the dynamic boundary condition with different ξ.

(δt,Resolution)	$\xi = 0.006$		$\xi = 0.008$		$\xi = 0.010$		$\xi = 0.012$	
	#Err	#Rate	#Err	#Rate	#Err	#Rate	#Err	#Rate
(1/1,8)	3.62E-2	0	3.92E-2	0	4.24E-2	0	4.25E-2	0
(1/2,16)	1.94E-2	0.90	2.00E-2	0.97	2.16E-2	0.98	2.31E-2	0.88
(1/4,32)	6.73E-3	1.52	7.95E-3	1.33	9.46E-3	1.19	1.08E-3	1.10
(1/8,64)	1.69E-3	1.99	2.85E-3	1.48	4.01E-3	1.24	5.16E-3	1.07
(1/16,128)	9.48E-4	0.83	9.16E-4	1.64	2.02E-3	0.99	3.09E-3	0.74

6.2. Wetting on chemically patterned surfaces

We then compute a wetting problem on a chemically pattern solid surface by our algorithm with $\xi = 0$. We assume the lower boundary Γ is composed of two materials with different Young's angles. Two typical material distributions are shown in Figure 5 and 7. We use $\mathcal{A}$ to represent the red parts and $\mathcal{B}$ to represent the green parts. Their corresponding Young's angles are respectively $\theta_{\mathcal{A}} = 2\pi/3$ and $\theta_{\mathcal{B}} = \pi/3$.

On the chemically patterned surface, We first give an initial droplet and perform our algorithm until a stable state is reached (i.e. the energy in (8) is minimized). After that, we increase(or decrease) the volume of the droplet a little by changing the level-set of the signed distance function slightly. The new droplet may not be stable. We use our algorithm again to compute a stable state. By repeating this process, we can observe the advancing(or receding) contact angle and the corresponding contact points. The difference between the advancing and receding trajectories gives the interesting contact angle hysteresis phenomena. More details will be given below.

We first consider the $k = 2$ case, which implies there are two green patterns in each side of the middle point on the lower surface as shown in Figure 5. The computational domain Ω is $(0, 1) \times (0, 1)$. We solve this problem on a uniform 256×256 spacial mesh and the time step is fixed at $\delta t = t_{unit}/40$. In the advancing case, the initial droplet has a circular surface with two contact points $(0.45, 0)$ and $(0.55, 0)$ which are located in the central red part. The initial contact angles are $\theta_1 = \theta_2 = \theta_{\mathcal{A}} = \frac{2}{3}\pi$. Since the local contact angles equal to Young's angle, the initial state of the droplet is stationary. We add some volume to the initial state and solve the problem (8) by using Algorithm 1 until we find a solution. We repeat the process again and again until the distance d of the contact points from the middle point $(0.5, 0)$ is larger than 0.35. In the process, the volume we added in each iteration is determined by the current position of the contact points. To be precise, let $2d$ be the distance between the two contact points, we add a volume of $\pi d^2/20$. In the receding case, the initial droplet is circular and has two contact points $(0.15, 0)$ and $(0.85, 0)$ which are located in the outer red parts on the chemically patterned boundary. We set the initial contact angles as $\theta_1 = \theta_2 = \theta_{\mathcal{A}} = \frac{2}{3}\pi$. In this case, we decrease the volume gradually. In each iteration, the volume we decrease is computed similarly as in the advancing case. We repeat this process until $d < 0.05$.

Figure 5 shows the position of the contact points(its distance d away from the middle point) and the contact angle θ with respect to the volume of the droplet. It is clear that contact angle hysteresis phenomena occur during the processes. Both the trajectories of the position of the contact point and the contact angles are different for the advancing(increasing volume) and receding(decreasing volume) cases. The hysteresis occurs near some joint points of the two materials. The largest advancing contact angle is equal to $\theta_{\mathcal{A}}$ and the smallest receding contact angle is equal to $\theta_{\mathcal{B}}$. The results are consistent with the analytical analysis in [11]. Figure 5 shows the drop profiles for different volumes in the advancing case. We see clearly the stick-slip phenomena of the contact points. In the receding case, the stick-slip behaviour of the droplet is similar to the advancing case.

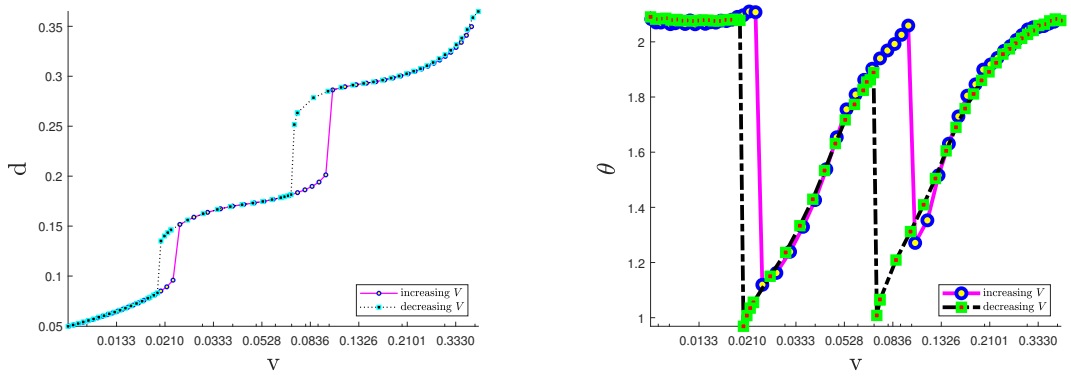

Figure 4: Contact angle hysteresis and constact line slipping($k = 2$). Contact point (left) moved and contact angles (right) varied by the changing of drop volume.

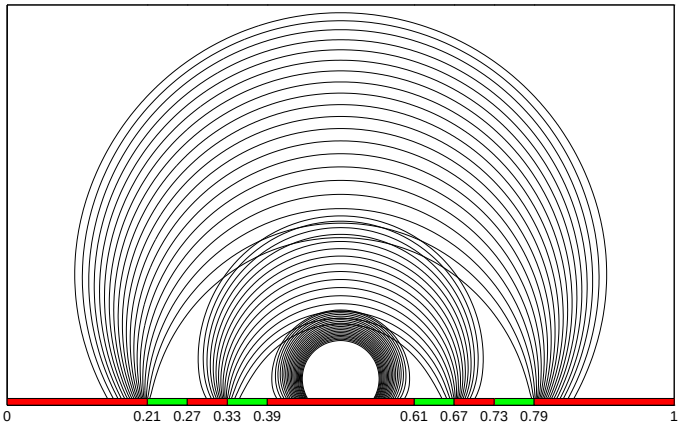

Figure 5: The drop profiles with increasing volume when $k = 2$.

In the $k = 4$ case, the patterned surface is shown as in Figure 7. Since there are more patterns on the lower boundary of $\Omega = (0, 1) \times (0, 1)$, we need finer meshes to resolve the chemical patterns. In our experiments, we adopt a 512×512 spacial mesh and the time step is chosen as $\delta t = t_{unit}/80$. We do similar computations as in the $k = 2$ case. The only difference is that the volume of the droplet changes more slowly. Suppose the current droplet has a circular surface with two contact points, which are of distance d away from the middle point of the lower boundary. The volume we add (decrease) in the advancing(receding) case is $\pi d^2/40$.

In Figure 6 and Figure 7, we draw the pictures of d and θ as functions of the volume v and the profiles

of drops for the case $k = 4$. The results are quite similar to the case $k = 2$. We observe the hysteresis in the trajectories of the contact angle and contact positions. There are also clear stick-slip phenomena of the contact points in the profile of the droplet. Since we have more patterns in this distribution of the materials on the substrate, we can see more stick-slip phenomena on the joint points of the two materials.

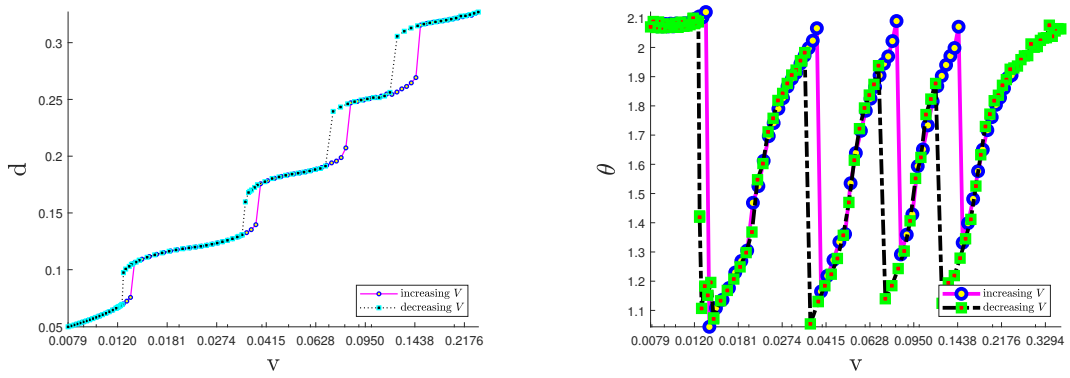

Figure 6: Contact angle hysteresis and constact line slipping($k = 4$). Contact point (left) moved and contact angles (right) varied by the changing of drop volume.

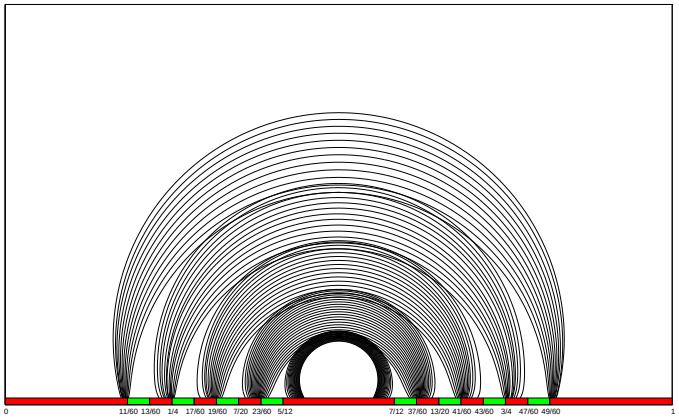

Figure 7: The drop profiles with increasing volume in the $k = 4$ case.

7. Conclusions and Further discussions

By using the Onsager principle as an approximation tool, we develop a new diffusion generated motion method for the wetting problem. The key idea is to consider the leading order approximation of a modified Allen-Cahn equation with a nonlinear relaxed boundary condition on a solid surface. By assuming the leading order has a *tanh* profile, we derive a linear diffusion equation for the signed distance function of the liquid-vapor interface. The equation is much simpler than the original phase field model and can act as a basis to construct our numerical method.

In the proposed method, we use the signed distance function to represent the interface between the liquid and vapor surface. In each iteration, only a linear diffusion equation with a linear boundary condition is solved, in addition to a re-distance step and a volume correction step. Numerical experiments show that the method has a convergence rate of $O(\delta t)$, which is much better than the previous threshold dynamics

method for wetting problems[12], where one can only obtain a half order $O(\delta t^{1/2})$ accuracy. The method can be seen as a generalization of the standard diffusion generate motion method using a signed distance function for mean curvature flows[25]. The energy stability of the method is analysed by careful studies for some geometric flows on the substrates. Numerical results show that the method works well for wetting on inhomogeneous surfaces.

In this paper, we focus on two-dimensional problems. Our method can be generalized to three-dimensional cases directly. For three dimensional problems, it is very helpful to use an adaptive spacial mesh to decrease the computational complexity as in [67].

Acknowledgement

We would like to thank Professor Dong Wang for helpful discussions. We also thank the anonymous referees for their valuable comments to help us to improve the paper. The work was partially supported by NSFC 11971469 and by the National Key R&D Program of China under Grant 2018YFB0704304 and Grant 2018YFB0704300.

A. Appendix: Further discussions on the geometric flows in Section 5.

In Theorem 5.1, we prove that the total energy decays after an iteration of geometric flows in Process 1 and Process 2 when the time step δt is small. In Proposition 5.2, we show that the constraint of the small time step can be removed when $\theta_Y = \frac{\pi}{2}$. We now try to extend the analysis in Proposition 5.2 to general cases when $\theta_Y \neq \pi/2$. It turns out the analysis is much more complicated and needs additional assumptions.

We introduce some notations. As shown in the Figure A.8, for a droplet with a surface $\mathcal{L}$ and a contact angle θ_Y on the two contact points a and b on the substrate, we can construct a domain D as follows: we draw radial straight lines oa and ob normal to the curve $\mathcal{L}$ at the points a and b and the two lines intersect at point o, then D is the domain enclosed by the curve $\mathcal{L}$ and the segments oa and ob. Obviously we have the angle $\angle aob = 2\theta_Y$. We set $L = |\mathcal{L}|$ and $L_{ab} = |ab|$. We also denote the area of D as $A_0 := |D|$ and the area of the original droplet is A(enclosed by $\mathcal{L}$ and the segment ab). We suppose that the curve $\mathcal{L}$ can be expressed as $\{\mathbf{X} = (x(\alpha), y(\alpha)), 0 \leq \alpha \leq 2\theta_Y\}$.

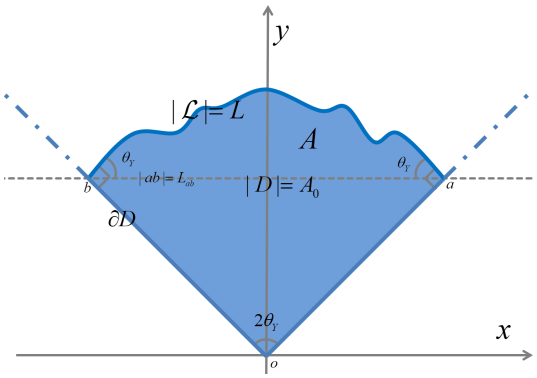

Figure A.8: The construction of a domain D

We first introduce some auxiliary geometric results with respect to the domain D. The first lemma is an isoperimetric inequality.

Lemma A.1. *Among all simple regular curves $\mathcal{L}$ as shown in the Figure A.8 with the same length L and the same contact angle θ_Y, the area A_0 of the domain D reaches its maximum when the curve is circular.*

Proof. The length of a curve is calculated as,

$$L = \int_0^{2\theta_Y} \sqrt{\left(\frac{\mathrm{d}x}{\mathrm{d}\alpha}\right)^2 + \left(\frac{\mathrm{d}y}{\mathrm{d}\alpha}\right)^2}\,\mathrm{d}\alpha$$

Applying the Green formula directly gives,

$$A_0 = \iint_D \mathrm{d}x\mathrm{d}y = \frac{1}{2}\int_{\partial D}(x\mathrm{d}y - y\mathrm{d}x) = \frac{1}{2}\int_0^{2\theta_Y}\left(x\frac{\mathrm{d}y}{\mathrm{d}\alpha} - y\frac{\mathrm{d}x}{\mathrm{d}\alpha}\right)\mathrm{d}\alpha - C_0$$

where $C_0 = \frac{1}{8}|b-a|^2\cot\theta_Y$. To maximize the area under the constraint of the length of the curve, we introduce a Lagrange multiplier λ and an energy functional J.

$$J = \frac{1}{2}\int_0^{2\theta_Y}\left(xy' - yx' + \lambda\sqrt{x'^2+y'^2} - \frac{C_0}{2\theta_Y}\right)\mathrm{d}\alpha.$$

We can derive its Euler Lagrangian equation as,

$$\begin{aligned}\tfrac{1}{2}y' &= \tfrac{\mathrm{d}}{\mathrm{d}\alpha}\left(-\tfrac{1}{2}y + \tfrac{\lambda x'}{\sqrt{x'^2+y'^2}}\right),\\ -\tfrac{1}{2}x' &= \tfrac{\mathrm{d}}{\mathrm{d}\alpha}\left(\tfrac{1}{2}x + \tfrac{\lambda y'}{\sqrt{x'^2+y'^2}}\right).\end{aligned}$$

The integral with respect to α leads to,

$$\begin{aligned}y &= \tfrac{\lambda x'}{\sqrt{x'^2+y^2}} + C_1,\\ x &= -\tfrac{\lambda y'}{\sqrt{x'^2+y^2}} + C_2,\end{aligned}$$

for some constants C_1 and C_2. Then we have,

$$(x-C_1)^2 + (y-C_2)^2 = \lambda^2.$$

Obviously, it represents a circular arc for $0 \le \alpha \le 2\theta_Y$. By computing the length of the curve, we can show that the Lagrange multiplier is $\lambda = \frac{L}{2\theta_Y}$ and the circular curve is given by

$$(x-C_1)^2 + (y-C_2)^2 = \left(\frac{L}{2\theta_Y}\right)^2.$$

The parameters C_1 and C_2 will correspond to the coordinates of the origin o. The proof is complete. □

The lemma is equivalent to the following geometric inequality for a domain D in Figure A.8:

$$\frac{L^2(t)}{A_0(t)} \ge 4\theta_Y, \tag{A.1}$$

where the equality holds if and only if $\mathcal{L}(t)$ is circular.

The next lemma is a Bonnesen type inequality for the domain D as in [68].

Lemma A.2. *For a simple regular curve $\mathcal{L}$ and a domain D as in Figure A.8, let $r_{in} = \min_\alpha |o - \mathbf{X}(\alpha)|$ and $r_{out} = \max_\alpha |o - \mathbf{X}(\alpha)|$. Then if r satisfies $r_{in} \le r \le r_{out}$, we have*

$$rL - A_0 - \theta_Y r^2 \ge 0. \tag{A.2}$$

The proof of the lemma follows the same line as the proof for the closed curves in [68]. It is quite cumbersome and we omit the proof for simplicity in presentation.

Recall the elastic energy of a curve is defined as $E = \frac{1}{2}\int_0^L \kappa^2 \, \mathrm{d}s$. The following conclusion is motivated by the analysis in [65].

Lemma A.3. *For a simple regular curve $\mathcal{L}$ and a domain D as in Figure A.8, if the droplet is convex, then we have*

$$A_0 E^2 \geq \theta_Y^3, \tag{A.3}$$

where the equality holds if and only if $\mathcal{L}$ is a circular curve.

Proof. Define $p(s) = \langle \mathbf{X}, -\mathbf{N} \rangle$ where $\mathbf{N}$ is the unit normal vector of $\mathcal{L}$ on $\mathbf{X}$.

$$\begin{aligned}\int_0^L p\kappa ds &= -\int_0^L \langle \mathbf{X}, \kappa \mathbf{N} \rangle \mathrm{d}s = -\int_0^L \langle \mathbf{X}, \mathbf{X}'' \rangle \, \mathrm{d}s \\ &= -\langle \mathbf{X}, \mathbf{X}' \rangle|_0^L + \int_0^L \langle \mathbf{X}', \mathbf{X}' \rangle \, \mathrm{d}s \\ &= L.\end{aligned}$$

The area of D is calculated as,

$$A_0 = \frac{1}{2}\int_0^L \langle \mathbf{X}, -\mathbf{N} \rangle \mathrm{d}s = \frac{1}{2}\int_0^L p \mathrm{d}s \tag{A.4}$$

Obviously, $r_{in} \leq p \leq r_{out}$ when the droplet is convex, then invoking Lemma A.2 yields

$$pL - A_0 - \theta_Y p^2 \geq 0.$$

Integral on both sides of the inequality, together with (A.4), we can readily get

$$\int_0^L p^2 \mathrm{d}s \leqslant \frac{LA}{\theta_Y}. \tag{A.5}$$

(A.5) together with Cauchy-Swartz inequality reveals that

$$L = \int_0^L p\kappa \mathrm{d}s \leq \left(\int_0^L p^2 \mathrm{d}s\right)^{1/2} \left(\int_0^L \kappa^2 \mathrm{d}s\right)^{1/2} \leq \left(\frac{LA}{\theta_Y}\right)^{1/2} \left(\int_0^L \kappa^2 \mathrm{d}s\right)^{1/2} \tag{A.6}$$

By combining (A.1) and (A.6), we can derive (A.3) and finish the proof. □

Remark A.1. *In this lemma, we prove an inequality for the elastic energy when the droplet is convex. The inequality is similar to that in Lemma 5.3. For the general case when the droplet is non-convex, the conclusion can be proved as in [63] and [64].*

With the above geometric inequalities, we can generalize the stability analysis in Proposition 5.2 to the cases when $\theta_Y \neq \frac{\pi}{2}$. Here we need some further assumptions.

Proposition A.1. *Under the assumptions of Theorem 5.1, if we further assume that $(L_{ab}(\kappa(a) + \kappa(b)) - 4\sin\theta_Y)\cos\theta_Y \leq 0$ where $\kappa(a)$ and $\kappa(b)$ are the curvature of the curve on the two end points, then we have*

$$\mathcal{E}_2 \leq \mathcal{E}_0,$$

for $\delta t > 0$ such that $L(t_1) > 0$.

Proof. The proof of the proposition follows the same line as for Proposition 5.2. We first construct an auxiliary mean curvature flow process as follows. We assume that $\tilde{\mathcal{L}}(t)$ is a shrinking circular curve in the way of mean curvature flow from t_0 to t_1 with contact angle $\theta \approx \theta_Y$ and the terminal length $\tilde{L}(t_1) = L(t_1)$. We use `tilde` superscripts to characterize the geometric quantities corresponding to $\widetilde{\mathcal{L}}(t)$, including $\widetilde{L}(t), \widetilde{A}(t), \tilde{A}_0(t), \tilde{\kappa}$ and the radius $\tilde{R}$. We calculate the variation of the total energy that

$$\tilde{\mathcal{E}}_0 - \tilde{\mathcal{E}}_1 = \gamma \int_{t_0}^{t_1} \int_0^{\tilde{L}(t)} \tilde{\kappa}^2 \, \mathrm{d}s \, \mathrm{d}t = \gamma \int_{t_0}^{t_1} \frac{2\theta_Y}{\tilde{R}} \, \mathrm{d}t = \gamma \int_{t_0}^{t_1} \frac{4\theta_Y^2}{\tilde{L}(t)} \, \mathrm{d}t =: \tilde{I} \tag{A.7}$$

Applying Lemma 5.1 with $v_n = \tilde{\kappa} = 1/\tilde{R}$ readily gives,

$$\frac{\mathrm{d}}{\mathrm{d}t}\tilde{L}(t) = -\int_0^{\tilde{L}} \tilde{\kappa}^2 \, \mathrm{d}s + (v_x(0) - v_x(L)) \cos\theta_Y = -\frac{2\theta_Y}{\tilde{R}} - \frac{2}{\tilde{R}\tan\theta_Y} = -\frac{2}{\tilde{R}}(\theta_Y + \cot\theta_Y) = -\frac{4\theta_Y}{\tilde{L}(t)}(\theta_Y + \cot\theta_Y).$$

Solving the ODE with the condition $\tilde{L}(t_1) = L(t_1)$, we have

$$\tilde{L}(t) = \sqrt{L\left(t_1\right)^2 + 8\theta_Y\left(\theta_Y + \cot\theta_Y\right)(t_1 - t)}.$$

This leads to

$$\tilde{I} = \gamma \int_{t_0}^{t_1} \frac{4\theta_Y^2}{\sqrt{L\left(t_1\right)^2 + 8\theta_Y\left(\theta_Y + \cot\theta_Y\right)(t_1 - t)}} \, \mathrm{d}t. \tag{A.8}$$

$\tilde{I}$ happens to be equal to II in Theorem 5.1. We need only to prove

$$\tilde{I} = \tilde{\mathcal{E}}_0 - \tilde{\mathcal{E}}_1 = \gamma \int_{t_0}^{t_1} \int_0^{\tilde{L}(t)} \tilde{\kappa}^2 \, \mathrm{d}s \, \mathrm{d}t \le \mathcal{E}_0 - \mathcal{E}_1 = \gamma \int_{t_0}^{t_1} \int_0^{L(t)} \kappa^2 \, \mathrm{d}s \, \mathrm{d}t = I.$$

It suffices to show that for any $t \in [t_0, t_1]$,

$$\tilde{E}(t) = \frac{1}{2}\int_0^{\tilde{L}(t)} \tilde{\kappa}^2 \, \mathrm{d}s \le \frac{1}{2}\int_0^{L(t)} \kappa^2 \, \mathrm{d}s = E(t). \tag{A.9}$$

We construct a domain D(with area A_0) as in Figure A.8 for a given droplet(with area A). By basic geometric relations,

$$\frac{\mathrm{d}(A_0 - A)}{\mathrm{d}t} = \frac{\mathrm{d}}{\mathrm{d}t}\left(\frac{L_{ab}^2}{4\tan\theta_Y}\right) = -\frac{L_{ab}(\kappa(a) + \kappa(b))}{2\sin\theta_Y \tan\theta_Y}.$$

Together with (34) we have

$$\frac{\mathrm{d}A_0}{\mathrm{d}t} = -2\theta_Y - \frac{L_{ab}(\kappa(a) + \kappa(b))}{2\sin\theta_Y \tan\theta_Y}.$$

In particular, for the circular case, we have

$$\frac{\mathrm{d}\tilde{A}_0}{\mathrm{d}t} = -2\theta_Y - \frac{4\sin\theta_Y}{2\sin\theta_Y\tan\theta_Y} = -2\theta_Y - \frac{2}{\tan\theta_Y}.$$

Under the condition that $\cos\theta_Y(L_{ab}(\kappa(a) + \kappa(b)) - 4\sin\theta_Y) \le 0$, we have

$$\frac{\mathrm{d}\tilde{A}_0}{\mathrm{d}t} \le \frac{\mathrm{d}A_0}{\mathrm{d}t}.$$

Together with Lemma A.1 that $\tilde{A}_0(t_1) \ge A_0(t_1)$ and the Leibniz formula, we can easily see that

$$\tilde{A}_0(t) - A_0(t) = \tilde{A}_0(t_1) - A_0(t_1) + \int_t^{t_1} \left(\frac{\mathrm{d}A_0}{\mathrm{d}t} - \frac{\mathrm{d}\tilde{A}_0}{\mathrm{d}t}\right)\mathrm{d}t \ge 0. \tag{A.10}$$

For any $t \in [t_0, t_1]$, we construct an auxiliary circular curve state $\check{\mathcal{L}}(t)$ with smaller radius $\check{R}$, and its related geometric quantity is represented by notations with the superscript $\texttt{check}(\check{})$. We set $\check{A}_0(t) = A_0(t)$. By (A.10), we have

$$\check{A}_0(t) \leq \tilde{A}_0(t). \tag{A.11}$$

And then applying definition of E to circular curve gives

$$\check{E}(t) = \frac{1}{2}\int_0^{\check{L}} \check{\kappa}^2 \, \mathrm{d}s = \frac{\theta_Y}{\check{R}(t)} = \frac{\theta_Y\sqrt{\theta_Y}}{\sqrt{\check{A}_0(t)}} \geq \frac{\theta_Y\sqrt{\theta_Y}}{\sqrt{\tilde{A}_0(t)}} = \tilde{E}(t). \tag{A.12}$$

Lemma A.3 reveals

$$E(t) \geq \check{E}(t). \tag{A.13}$$

It together with (A.12) implies (A.9). This ends the proof. □

Remark A.2. *This assumption* $(L_{ab}(\kappa(a)+\kappa(b)) - 4\sin\theta_Y)\cos\theta_Y \leq 0$ *is an additional condition needed in the analysis. It holds naturally in some cases,, e.g. when the curve* $\mathcal{L}$ *is circular so that* $L_{ab}(\kappa(a)+\kappa(b)) = 4\sin\theta_Y$ *or when* $\theta_Y = \frac{\pi}{2}$*. The later case is consistent with the analysis in Proposition 5.2. It is remarkable that a circular curve satisfies the condition, since this indicates there is not restriction on the time step when a droplet approaches to its stationary state. Then a large time step can be used for long time simulations. (Nevertheless, the large time step might affect accuracy of the method.) In other cases, the assumption implies some constraint on the length* L_{ab} *and the curvatures* $\kappa(a)$ *and* $\kappa(b)$*, which might be needed for the energy decay property.*

References

[1] T. Young. An essay on the cohesion of fluids. Philos. Trans. R. Soc. London, 95:65–87, 1805.
[2] P.G. de Gennes. Wetting: Statics and dynamics. Rev. Mod. Phys., 57:827–863, 1985.
[3] D. Bonn, J. Eggers, J. Indekeu, J. Meunier, and E. Rolley. Wetting and spreading. Rev. Mod. Phys., 81:739–805, 2009.
[4] P.G. de Gennes, F. Brochard-Wyart, and D. Quere. Capillarity and Wetting Phenomena. Springer Berlin, 2003.
[5] W. Ren. Wetting transition on patterned surfaces: transition states and energy barriers. Langmuir, 30:2879–2885, 2014.
[6] K. Deckelnick, G. Dziuk, and C. M. Elliott. Computation of geometric partial differential equations and mean curvature flow. Acta numerica, 14:139–232, 2005.
[7] K. A. Brakke. The surface evolver. Exp. math., 1(2):141–165, 1992.
[8] D. E. Womble. A front-tracking method for multiphase free boundary problems. SIAM J. Numer. Anal., 26(2):380–396, 1989.
[9] H. Zhao, T. Chan, B. Merriman, and S. J. Osher. A variational level set approach to multiphase motion. J. Comput. Phys., 127(1):179–195, 1996.
[10] T. Qian, X.-P. Wang, and P. Sheng. Molecular scale contact line hydrodynamics of immiscible flows. Phy. Rev. E, 68(1):016306–15, July 2003.
[11] X. Xu and X. P. Wang. Analysis of wetting and contact angle hysteresis on chemically patterned surfaces. SIAM J. Appl. Math., 71:1753–1779, 2011.
[12] X. Xu, D. Wang, and X.-P. Wang. An efficient threshold dynamics method for wetting on rough surfaces. J. Comput. Phys., 330:510–528, 2017.
[13] D. Wang, X. Xu, and X.-P. Wang. An improved threshold dynamics method for wetting dynamics. J. Comput. Phys., 392:291–310, 2019.
[14] S. Jiang, D. Wang, and X. P. Wang. An efficient boundary integral scheme for the MBO threshold dynamics method via the NUFFT. J. Sci. Comput., 74:474–490, 2018.
[15] D. Wang, S. Jiang, and X.-P. Wang. An efficient boundary integral scheme for the threshold dynamics method ii: Applications to wetting dynamics. J. Sci. Comp., 81(3):1860–1881, 2019.
[16] B. Merriman, J. K. Bence, and S. Osher. Diffusion generated motion by mean curvature. UCLA CAM Report 92-18, 1992.
[17] S. J. Ruuth. Efficient algorithms for diffusion-generated motion by mean curvature. J. Comput. Phys., 144(2):603–625, 1998.
[18] S. J. Ruuth. A diffusion-generated approach to multiphase motion. J. Comput. Phys., 145(1):166–192, 1998.
[19] S. Esedoglu and F. Otto. Threshold dynamics for networks with arbitrary surface tensions. Comm. Pure Appl. Math., 2015.
[20] Steven J Ruuth and Barry Merriman. Convolution–thresholding methods for interface motion. J. Computat. Phys., 169(2):678–707, 2001.

[21] S. Esedoglu and R. Tsai. Threshold dynamics for the piecewise constant Mumford–shah functional. J. Comput. Phys., 211(1):367–384, 2006.
[22] D. Wang, H. Li, X. Wei, and X.-P. Wang. An efficient iterative thresholding method for image segmentation. J. Comput. Phys., 350:657–667, 2017.
[23] M. Elsey and S. Esedoglu. Threshold dynamics for anisotropic surface energies. Math. Comp., 87(312):1721–1756, 2018.
[24] B. Osting and D. Wang. A diffusion generated method for orthogonal matrix-valued fields. Math. Comp., 2019, DOI:https://doi.org/10.1090/mcom/3473.
[25] S. Esedoglu, S. Ruuth, and R. Tsai. Diffusion generated motion using signed distance functions. J. Comput. Phys., 229(4):1017–1042, 2010.
[26] C. Kublik, S. Esedoglu, and J. A. Fessler. Algorithms for area preserving flows. SIAM J. Sci. Comput., 33(5):2382–2401, 2011.
[27] A. Zaitzeff, S. Esedoglu, and K. Garikipati. On the voronoi implicit interface method. SIAM J. Sci. Comput., 41(4):A2407–A2429, 2019.
[28] A. Zaitzeff, S. Esedoglu, and K. Garikipati. Second order threshold dynamics schemes for two phase motion by mean curvature. J. Comput. Phys., page 109404, 2020.
[29] L. Onsager. Reciprocal relations in irreversible processes. II. Phys. Rev., 38(12):2265–2279, dec 1931.
[30] L.Onsager. Reciprocal relations in irreversible processes. I. Phys. Rev., 37(4):405–426, feb 1931.
[31] M. Doi. Soft Matter Physics. Oxford University Press, Oxford, 2013.
[32] M. Doi. Onsager principle as a tool for approximation. Chin. Phys. B, 24:020505, 2015.
[33] X. Xu, Y. Di, and M. Doi. Variational method for contact line problems in sliding liquids. Phys. Fluids, 28:087101, 2016.
[34] Y. Di, X. Xu, and M. Doi. Theoretical analysis for meniscus rise of a liquid contained between a flexible film and a solid wall. Europhys. Lett., 113(3):36001, feb 2016.
[35] Xingkun Man and Masao Doi. Ring to mountain transition in deposition pattern of drying droplets. Phys. Rev. Lett., 116:066101, 2016.
[36] J. Zhou, Y. Jiang, and M. Doi. Cross interaction drives stratification in drying film of binary colloidal mixtures. Phys. Rev. Lett., 118:108002, 2017.
[37] Y. Di, X. Xu, J. Zhou, and M. Doi. Analysis of thin film dynamics in coating problems using Onsager principle. Chin. Phys. B, 27(2):024501, 2018.
[38] S. Guo, X. Xu, T. Qian, Y. Di, M. Doi, and P. Tong. Onset of thin film meniscus along a fibre. J. Fluid Mech., 865:650–680, 2019.
[39] W. Jiang, Q. Zhao, T. Qian, D. J. Srolovitz, and W. Bao. Application of Onsager's variational principle to the dynamics of a solid toroidal island on a substrate. Acta Mater., 163:154–160, 2019.
[40] M. Doi. Onsager's variational principle in soft matter. J. Phys.: Condens. Matter, 23:284118, 2011.
[41] T. Qian, X.-P. Wang, and P. Sheng. A variational approach to moving contact line hydrodynamics. J. Fluid Mech., 564:333–360, 2006.
[42] L Modica and S Mortola. Il limite nella gamma-convergenza di una famiglia di funzionali ellittici. Boll. Math. Ital. A, 14, 1977.
[43] L. Modica. Gradient theory of phase transitions with boundary contact energy. In Annales de l'Institut Henri Poincare (C) Non Linear Analysis, volume 4, pages 487–512. Elsevier, 1987.
[44] X. Chen, X.-P. Wang, and X. Xu. Analysis of the Cahn-Hilliard equation with relaxation boundary condition modelling contact angle. Arch. Rational Mech. Anal., 213:1–24, 2014.
[45] C. G. Gal and M. Grasselli. The non-isothermal allen-cahn equation with dynamic boundary conditions. Disc. Cont. Dyn. Sys.-A, 22(4):1009, 2008.
[46] J. Sprekels and H. Wu. A note on parabolic equation with nonlinear dynamical boundary condition. Nonlinear Analysis: Theory, Methods & Applications, 72(6):3028–3048, 2010.
[47] L. Calatroni and P. Colli. Global solution to the allen–cahn equation with singular potentials and dynamic boundary conditions. Nonlinear Analysis: Theory, Methods & Applications, 79:12–27, 2013.
[48] Pierluigi Colli and Takeshi Fukao. The allen–cahn equation with dynamic boundary conditions and mass constraints. Math. Methods Appl. Sci., 38(17):3950–3967, 2015.
[49] Makoto Okumura and Daisuke Furihata. A structure-preserving scheme for the allen–cahn equation with a dynamic boundary condition. Disc. Cont. Dyn. Sys.-A, 40(8):4927, 2020.
[50] W. Jiang, W. Bao, C. V. Thompson, and D. J. Srolovitz. Phase field approach for simulating solid-state dewetting problems. Acta materialia, 60(15):5578–5592, 2012.
[51] J. Shen and X. Yang. Numerical pproximations of allen-cahn and cahn-hilliard equations. Discrete Contin. Dyn. Syst. B, 28(4):1669–1691, 2010.
[52] Q. Du and X. Feng. The phase field method for geometric moving interfaces and their numerical approximations. Geometric Partial Differential Equations-Part I, Handbook of Numerical Analysis, 21, 2020.
[53] G. Caginalp and P. C. Fife. Dynamics of layered interfaces arising from phase boundaries. SIAM J. Appl. Math., 48(3):506–518, 1988.
[54] J. A. Sethian. Level set methods and fast marching methods: evolving interfaces in computational geometry, fluid mechanics, computer vision, and materials science, volume 3. Cambridge university press, 1999.
[55] G. Russo and P. Smereka. A remark on computing distance functions. J. Comput. Phys., 163(1):51–67, 2000.
[56] S. Osher and R. P. Fedkiw. Level set methods: an overview and some recent results. J. Comput. Phy., 169(2):463–502, 2001.
[57] L. Cheng and Y. Tsai. Redistancing by flow of time dependent eikonal equation. J. Comput. Phys., 227(8):4002–4017,

2008.
[58] M. Elsey and S. Esedoglu. Fast and accurate redistancing by directional optimization. SIAM J. Sci. Comput., 36(1):A219–A231, 2014.
[59] S. J Ruuth and B. T. Wetton. A simple scheme for volume-preserving motion by mean curvature. J. Sci. Comput., 19(1-3):373–384, 2003.
[60] K. Svadlenka, E. Ginder, and S. Omata. A variational method for multiphase volume-preserving interface motions. J. Comput. Appl. Math., 257:157–179, 2014.
[61] R. Kimmel. Numerical geometry of images: Theory, algorithms, and applications. Springer Science & Business Media, 2003.
[62] Andrew N Pressley. Elementary differential geometry. Springer Science & Business Media, 2010.
[63] Vincenzo Ferone, Bernd Kawohl, and Carlo Nitsch. The elastica problem under area constraint. Mathematische Annalen, 365(3-4):987–1015, 2016.
[64] Dorin Bucur and Antoine Henrot. A new isoperimetric inequality for the elasticae. Journal of the European Mathematical Society, 19(11):3355–3376, 2017.
[65] Michael E Gage. An isoperimetric inequality with applications to curve shortening. Duke Mathematical Journal, 50(4):1225–1229, 1983.
[66] Michael E Gage. Curve shortening makes convex curves circular. Inventiones mathematicae, 76(2):357–364, 1984.
[67] X. Xu and W.-J. Ying. An adaptive threshold dynamics method for three-dimensional wetting on rough surfaces. Comm. Comput. Phys., to appear, 2020.
[68] Robert Osserman. Bonnesen-style isoperimetric inequalities. The American Mathematical Monthly, 86(1):1–29, 1979.